vagotomy abolished the anorectic effect of PYY3-36. Similarly, the anorectic effects of peripheral GLP-1 administration were also abolished by vagotomy [46]. Thus, peripheral PYY3-36 and GLP-1 transmit satiety signals to the brain via the vagal afferent pathway. On the other hand, ghrelin is a peptide recently found to be produced in the stomach, which acts on a previously identified orphan receptor (growth hormone secretagogue receptor), activation of which in the hypothalamus causes growth hormone (GH) release from the pituitary gland [50]. Date *et al.* [47] reported blockade of the gastric vagal afferent to abolish ghrelin-induced feeding, GH secretion and the activations of NPY- and GHRH-producing neurons. The ghrelin receptor is also expressed in vagal afferent terminals, and ghrelin suppresses vagal afferent firing. Taken together, these findings indicate involvement of gastric vagal afferent in conveying signals regarding satiety as well as starvation from the gut to the brain.

b) Signals from the liver — Liver functions as an energy balance sensor —

(1) Hepatoportal glucose sensor

Nutrients absorbed from the gut enter the portal vein, and thereby reach the liver directly. Therefore, given its anatomical location, it seems reasonable that the liver functions as a glucose sensor. It has been demonstrated that signals regarding serum glucose levels from the so-called hepatoportal glucose sensor to the brain are carried along afferent vagal nerve pathways [40]. The hepatoportal glucose sensor, which is an as yet incompletely defined structure, is activated by a glucose gradient established between the portal vein and the periphery. Raising portal vein glucose levels leads to a decrease in vagal afferent discharges reaching the nuclei of solitary tract neurons, leading to activation of sympathetic efferents to the adrenal glands, liver, splanchnic bed and pancreas. Because all of these reflex efferent outputs are blocked by hepatic vagotomy, it appears that signals triggered by high levels of portal glucose are transmitted through vagal afferents [51, 52]. Burcelin *et al.* showed that the hepatoportal sensor requires the presence of GLUT2 but that hepatocytes are not involved in this sensing process [53], in agreement with previous studies showing this sensor to be located upstream from the hepatic hylus [54]. They also reported that GLP-1 signaling modulates hepatoportal glucose sensing [55], an observation compatible with the role of GLP-1 in regulating the firing activity of hepatic vagal afferents [56]. A similar role for GLP-1 in canine hepatoportal sensor function has also been reported [57].

On the other hand, sympathetic afferents mediate hypoglycemic signals. Reportedly, a counterregulatory response to moderate systemic hypoglycemia, *i.e.* sympathetic efferent activation, is attenuated by clamping the liver at euglycemic levels and is disrupted by interruption of sympathetic (but not vagal) afferents from the hepatic portal circulation [58, 59]. Collectively, these observations indicate that the afferent autonomic nervous system, including both vagal and sympathetic nerves, from the hepatoportal structure, plays important roles in conveying information regarding peripheral glucose levels to the brain.

(2) PPARγ (peroxisome proliferator-activated receptor γ)

Recently, in a number of studies, tissue-specific knockout mice have been found to exhibit unexpected phenotypes, suggesting the presence of as yet unknown cross-talk between organs/tissues. Therefore, unraveling the complexities of this inter-organ communication would be very important for elucidating the mechanisms underlying not only energy and glucose homeostasis but also the development of obesity-related diseases. However, using genetically engineered mice, it is somewhat difficult to demonstrate the underlying mechanisms, since a substantial number of compensatory mechanisms can modify metabolic phenotypes. Alternatively, using adenoviral gene transfer into an organ/tissue of an adult mouse model, we observed an example of such inter-tissue communication; dissipating excess energy in the liver affects insulin sensitivity in muscle and adipose tissues [60]. Therefore, we suspected that, if metabolism could be altered in just one organ, it would be easier to analyze acute metabolic effects in other remote tissues and, assuming intervention to be possible, it would give us an understanding of the mechanisms.

Mice with tissue-specific knockout of peroxisome proliferator-activated receptor γ (PPARγ) may provide an example of such inter-tissue communication. Notably, liver-specific disruption of PPARγ in ob/ob mice prevented hepatic steatosis, but increased peripheral adiposity and decreased insulin sensitivity in muscle and adipose tissue [61]. Hepatic expression of PPARγ, especially PPARγ2, is functionally enhanced in a number of obesity models [62, 63]. Therefore, to unravel the mechanism underlying this inter-organ/tissue com-

munication between the liver and peripheral tissues including muscle and fat, we overexpressed PPARγ2 in the livers of mice using adenoviral gene transfer.

Hepatic PPARγ2 expression acutely induced severe hepatic steatosis, while peripheral adiposity was markedly reduced due to enhanced lipolysis. Systemic metabolic rates were increased and, therefore, peripheral insulin sensitivity and glucose tolerance showed marked improvement. Thus, hepatic expression of PPARγ2 exerts not only local effects in the liver, but also remote effects in adipose tissues and the whole body. These remote effects were explained by increased sympathetic outflow into muscle and adipose tissues. Therefore, to examine the possibility that afferent nerves originating in the liver are involved in the observed effects on energy expenditure and peripheral adiposity through efferent sympathetic nerve activation, we interrupted liver-brain communication by performing selective hepatic branch vagotomy. This manipulation significantly reversed the both reduction in peripheral adiposity and the enhancement of energy expenditure. In addition, pharmacological deafferentation of the vagus blocked the hepatic PPARγ2 expression-induced decrease in white adipose tissue weights. These findings indicate that hepatic PPARγ2 expression and/or hepatic lipid accumulation stimulate afferent vagal nerve fibers, communicating metabolic information to the brain, leading to anti-obesity and anti-insulin-resistant effects in muscle and adipose tissue [64].

Fat storage in the liver changes dynamically according to the systemic energy balance and is associated with several features of the metabolic syndrome. Since hepatic PPARγ expression is physiologically associated with obesity, the liver may convey information regarding excess energy to the central nervous system via the afferent vagus. This neuronal system is likely to underlie chronic "adaptive thermogenesis", resulting in protection against metabolic perturbation induced by excessive energy storage (Fig. 3). When the brain obtains information regarding excess energy storage mediated by leptin from adipose tissues and via the afferent vagus from the liver, the sympathetic nervous system is activated to enhance energy expenditure and lipolysis, thereby maintaining energy homeostasis.

c) Signals from adipose tissues

There are only a few reports focusing on afferent nerve signals from adipose tissue. According to these reports, activation of afferent nerves from intra-abdominal (epididymal) adipose tissue resulted in reflex signals being sent to white adipose tissues via efferent sympathetic nerve activation [36, 37]. However, the functional significance of these afferent signals was unclear. We demonstrated hypothalamic leptin sensitivity to be modulated through afferent nerves from epididymal fat [39].

Fat accumulation in intra-abdominal fat tissue plays a major role in development of the metabolic syndrome associated with insulin and leptin resistance. Leptin resistance is induced by excessive adiposity and, in turn, is an important mechanism underlying maintenance of the obese state. To determine whether a local reduction in the adiposity of intra-abdominal adipose tissue of diabetic mice with diet-induced obesity would reverse obesity-related metabolic disorders, in particular insensitivity to leptin and insulin, we attempted to express uncoupling protein-1 (UCP1), which functions to dissipate energy as heat. UCP1 was expressed in epididymal adipose tissue only at very low levels. Nevertheless, food intake declined in association with decreased serum leptin levels as well as downregulation of the orexigenic neuropeptide Y and upregulation of the anorexigenic precursour neuropeptide proopiomelanocortin, in the hypothalamus. The anorectic response to exogenous leptin was enhanced by adipose UCP1 expression. In addition, the hypophagia could not be duplicated in db/db mice with mutant leptin receptors. Collectively, these findings clearly show that very limited UCP1 expression in the intra-abdominal fat pad dramatically improves hypothalamic leptin resistance. Local dissection of nerves from the epididymal fat pad and pharmacological deafferentation blunted the anorectic effects of UCP1 expression in adipose tissue. Taken together, the results suggest afferent nerve signals originating in epididymal fat pads to modulate hypothalamic sensitivity to leptin (Fig. 4).

Adipose tissues were long regarded as a simply being passive fuel storage sites. However, the discovery of various adipocytokines, with leptin being the most important example, has raised adipose tissue to the status of a versatile endocrine gland. Recent studies including ours provide further evidence of the key role of adipose tissue as a base from which neuronal signals regulating feeding and fuel metabolism are sent. Furthermore, identification of the neurotransmitted

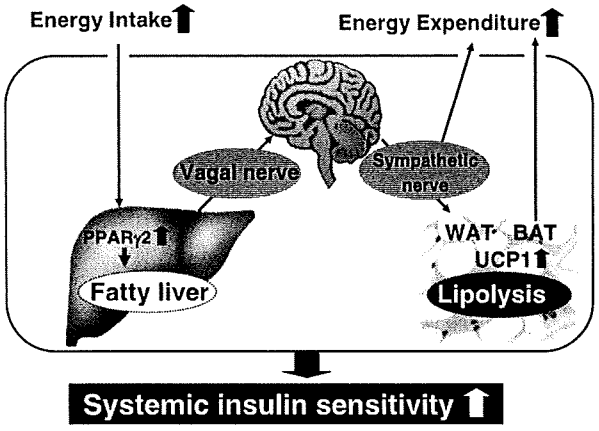

Fig. 3. Scheme of the neuronal pathway originating in the liver. Hepatic PPARγ expression associated with surplus energy results in increased energy expenditure, decreased peripheral adiposity and improved insulin sensitivity via the neuronal system consisting of afferent vagal and efferent sympathetic nerves.

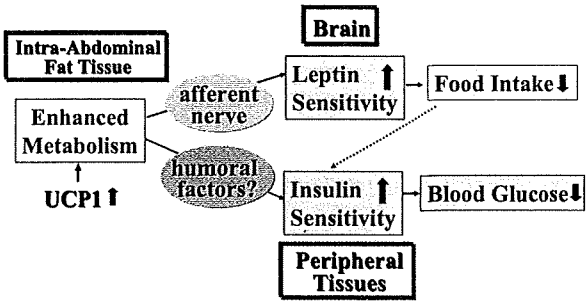

Fig. 4. The proposed mechanism whereby UCP1 expression in epididymal fat tissue decreases food intake and improves glucose tolerance (quoted from [39] with slight modification).

substance involved might lead to development of novel therapeutic strategies aimed at tackling the metabolic syndrome.

Conclusion

Metabolism does not go on independently in different organs/tissues, but rather in a coordinated and regulated manner throughout the body. Metabolic regulation coordinated among organs/tissues, which requires communication among these organs/tissues, appears to be essential for maintaining the homeostasis of systemic metabolism, in particular glucose and energy metabolism. In addition, disturbance of this coordinated control system may be implicated in the development of metabolic disorders, such as obesity, type 2 diabetes, hyperlipidemia and the metabolic syndrome.

Recent advances in this field revealed the complex and important roles of the central nervous system. The brain obtains a variety of metabolic information from peripheral organs/tissues through humoral and neuronal avenues. These inputs are likely to be integrated and processed in the brain, leading to the transmission of regulatory signals, which induce appropriate metabolic responses, throughout the body. Further elucidation of these regulatory systems, in much greater detail, may allow us to unravel the mechanisms underlying metabolic homeostasis and thereby to understand the metabolic disorders. Moreover, targeting of these neuronal pathways is a potential therapeutic strategy for the metabolic syndrome.

References

1. Flier JS (2004) Obesity wars: molecular progress confronts an expanding epidemic. *Cell* 116: 337–350.
2. Miller JC, Gnaedinger JM, Rapoport SI (1987) Utilization of plasma fatty acid in rat brain: distribution of [14C]palmitate between oxidative and synthetic pathways. *J Neurochem* 49: 1507–1514.
3. Rapoport SI (1996) In vivo labeling of brain phospholipids by long-chain fatty acids: relation to turnover and function. *Lipids* 31 (Suppl): S97–101.
4. Wang R, *et al.* (2006) Effects of oleic acid on distinct populations of neurons in the hypothalamic arcuate nucleus are dependent on extracellular glucose levels. *J Neurophysiol* 95: 1491–1498.
5. Obici S, *et al.* (2002) Central administration of oleic acid inhibits glucose production and food intake. *Diabetes* 51: 271–275.
6. Obici S, *et al.* (2003) Inhibition of hypothalamic carnitine palmitoyltransferase-1 decreases food intake and glucose production. *Nat Med* 9: 756–761.
7. Pocai A, *et al.* (2005) A brain-liver circuit regulates glucose homeostasis. *Cell Metab* 1: 53–61.
8. Hu Z, *et al.* (2003) Hypothalamic malonyl-CoA as a mediator of feeding behavior. *Proc Natl Acad Sci USA* 100: 12624–12629.

9. Minokoshi Y, *et al.* (2004) AMP-kinase regulates food intake by responding to hormonal and nutrient signals in the hypothalamus. *Nature* 428: 569–574.
10. Andersson U, *et al.* (2004) AMP-activated protein kinase plays a role in the control of food intake. *J Biol Chem* 279: 12005–12008.
11. Choi YH, Fletcher PJ, Anderson GH (2001) Extracellular amino acid profiles in the paraventricular nucleus of the rat hypothalamus are influenced by diet composition. *Brain Res* 892: 320–328.
12. Cota D, *et al.* (2006) Hypothalamic mTOR signaling regulates food intake. *Science* 312: 927–930.
13. Meijer AJ, Dubbelhuis PF (2004) Amino acid signalling and the integration of metabolism. *Biochem Biophys Res Commun* 313: 397–403.
14. Proud CG (2002) Regulation of mammalian translation factors by nutrients. *Eur J Biochem* 269: 5338–5349.
15. Levin BE, *et al.* (2004) Neuronal glucosensing: what do we know after 50 years? *Diabetes* 53: 2521–2528.
16. Arluison M, *et al.* (2004) Distribution and anatomical localization of the glucose transporter 2 (GLUT2) in the adult rat brain — an immunohistochemical study. *J Chem Neuroanat* 28: 117–136.
17. Arluison M, *et al.* (2004) Immunocytochemical localization of the glucose transporter 2 (GLUT2) in the adult rat brain. II. Electron microscopic study. *J Chem Neuroanat* 28: 137–146.
18. Sutherland VL, *et al.* (2005) Developmental expression of glucokinase in rat hypothalamus. *Brain Res Dev Brain Res* 154: 255–258.
19. Alvarez E, *et al.* (2005) The expression of GLP-1 receptor mRNA and protein allows the effect of GLP-1 on glucose metabolism in the human hypothalamus and brainstem. *J Neurochem* 92: 798–806.
20. Kang L, *et al.* (2004) Physiological and molecular characteristics of rat hypothalamic ventromedial nucleus glucosensing neurons. *Diabetes* 53: 549–559.
21. Wang R, *et al.* (2004) The regulation of glucose-excited neurons in the hypothalamic arcuate nucleus by glucose and feeding-relevant peptides. *Diabetes* 53: 1959–1965.
22. Prodi E, Obici S (2006) Minireview: the brain as a molecular target for diabetic therapy. *Endocrinology* 147: 2664–2669.
23. Plum L, Belgardt BF, Bruning JC (2006) Central insulin action in energy and glucose homeostasis. *J Clin Invest* 116: 1761–1766.
24. Pocai A, *et al.* (2005) Hypothalamic K(ATP) channels control hepatic glucose production. *Nature* 434: 1026–1031.
25. Inoue H, *et al.* (2006) Role of hepatic STAT3 in brain-insulin action on hepatic glucose production. *Cell Metab* 3: 267–275.
26. Friedman JM, Halaas JL (1998) Leptin and the regulation of body weight in mammals. *Nature* 395: 763–770.
27. Bates SH, Myers MG (2004) The role of leptin — STAT3 signaling in neuroendocrine function: an integrative perspective. *J Mol Med* 82: 12–20.
28. Bjorbaek C, *et al.* (1997) Divergent signaling capacities of the long and short isoforms of the leptin receptor. *J Biol Chem* 272: 32686–32695.
29. Niswender KD, *et al.* (2001) Intracellular signalling. Key enzyme in leptin-induced anorexia. *Nature* 413: 794–795.
30. Qi Y, *et al.* (2004) Adiponectin acts in the brain to decrease body weight. *Nat Med* 10: 524–529.
31. Badman MK, Flier JS (2005) The gut and energy balance: visceral allies in the obesity wars. *Science* 307: 1909–1914.
32. Shimazu T (1981) Central nervous system regulation of liver and adipose tissue metabolism. *Diabetologia* 20 (Suppl): 343–356.
33. Bartness TJ, Bamshad M (1998) Innervation of mammalian white adipose tissue: implications for the regulation of total body fat. *Am J Physiol* 275 (5 Pt 2): R1399–1411.
34. Imai J, *et al.* (2006) Cold exposure suppresses serum adiponectin levels through sympathetic nerve activation in mice. *Obesity (Silver Spring)* 14: 1132–1141.
35. Kreier F, *et al.* (2002) Selective parasympathetic innervation of subcutaneous and intra-abdominal fat — functional implications. *J Clin Invest* 110: 1243–1250.
36. Niijima A (1998) Afferent signals from leptin sensors in the white adipose tissue of the epididymis, and their reflex effect in the rat. *J Auton Nerv Syst* 73: 19–25.
37. Tanida M, *et al.* (2000) Leptin injection into white adipose tissue elevates renal sympathetic nerve activity dose-dependently through the afferent nerves pathway in rats. *Neurosci Lett* 293: 107–110.
38. Kreier F, *et al.* (2006) Tracing from fat tissue, liver, and pancreas: a neuroanatomical framework for the role of the brain in type 2 diabetes. *Endocrinology* 147: 1140–1147.
39. Yamada T, *et al.* (2006) Signals from intra-abdominal fat modulate insulin and leptin sensitivity through different mechanisms: neuronal involvement in food-intake regulation. *Cell Metab* 3: 223–229.
40. Thorens B, Larsen PJ (2004) Gut-derived signaling molecules and vagal afferents in the control of glucose and energy homeostasis. *Curr Opin Clin Nutr Metab Care* 7: 471–478.
41. Strader AD, Woods SC (2005) Gastrointestinal hormones and food intake. *Gastroenterology* 128: 175–191.
42. Havel PJ (2001) Peripheral signals conveying metabolic information to the brain: short-term and long-term regulation of food intake and energy homeostasis. *Exp Biol Med (Maywood)* 226: 963–977.
43. Kojima M, Kangawa K (2005) Ghrelin: structure and function. *Physiol Rev* 85: 495–522.

44. Smith GP, *et al.* (1981) Abdominal vagotomy blocks the satiety effect of cholecystokinin in the rat. *Science* 213: 1036–1037.
45. Koda S, *et al.* (2005) The role of the vagal nerve in peripheral PYY3-36-induced feeding reduction in rats. *Endocrinology* 146: 2369–2375.
46. Abbott CR, *et al.* (2005) The inhibitory effects of peripheral administration of peptide YY(3-36) and glucagon-like peptide-1 on food intake are attenuated by ablation of the vagal-brainstem-hypothalamic pathway. *Brain Res* 1044: 127–131.
47. Date Y, *et al.* (2002) The role of the gastric afferent vagal nerve in ghrelin-induced feeding and growth hormone secretion in rats. *Gastroenterology* 123: 1120–1128.
48. Reimann F, Gribble FM (2002) Glucose-sensing in glucagon-like peptide-1-secreting cells. *Diabetes* 51: 2757–2763.
49. Gribble FM, *et al.* (2003) A novel glucose-sensing mechanism contributing to glucagon-like peptide-1 secretion from the GLUTag cell line. *Diabetes* 52: 1147–1154.
50. Kojima M, *et al.* (1999) Ghrelin is a growth-hormone-releasing acylated peptide from stomach. *Nature* 402: 656–660.
51. Adachi A, *et al.* (1984) Convergence of hepatoportal glucose-sensitive afferent signals to glucose-sensitive units within the nucleus of the solitary tract. *Neurosci Lett* 46: 215–218.
52. Niijima A (1984) Reflex control of the autonomic nervous system activity from the glucose sensors in the liver in normal and midpontine-transected animals. *J Auton Nerv Syst* 10: 279–285.
53. Burcelin R, Dolci W, Thorens B (2000) Glucose sensing by the hepatoportal sensor is GLUT2-dependent: in vivo analysis in GLUT2-null mice. *Diabetes* 49: 1643–1648.
54. Hevener AL, Bergman RN, Donovan CM (1997) Novel glucosensor for hypoglycemic detection localized to the portal vein. *Diabetes* 46: 1521–1525.
55. Burcelin R, *et al.* (2001) Glucose competence of the hepatoportal vein sensor requires the presence of an activated glucagon-like peptide-1 receptor. *Diabetes* 50: 1720–1728.
56. Nakabayashi H, *et al.* (1996) Vagal hepatopancreatic reflex effect evoked by intraportal appearance of tGLP-1. *Am J Physiol* 271 (5 Pt 1): E808–813.
57. Ionut V, *et al.* (2005) Synergistic effect of portal glucose and glucagon-like peptide-1 to lower systemic glucose and stimulate counter-regulatory hormones. *Diabetologia* 48: 967–975.
58. Donovan CM, Halter JB, Bergman RN (1991) Importance of hepatic glucoreceptors in sympathoadrenal response to hypoglycemia. *Diabetes* 40: 155–158.
59. Fujita S, Donovan CM (2005) Celiac-superior mesenteric ganglionectomy, but not vagotomy, suppresses the sympathoadrenal response to insulin-induced hypoglycemia. *Diabetes* 54: 3258–3264.
60. Ishigaki Y, *et al.* (2005) Dissipating excess energy stored in the liver is a potential treatment strategy for diabetes associated with obesity. *Diabetes* 54: 322–332.
61. Matsusue K, *et al.* (2005) Liver-specific disruption of PPARgamma in leptin-deficient mice improves fatty liver but aggravates diabetic phenotypes. *J Clin Invest* 111: 737–747.
62. Rahimian R, *et al.* (2001) Hepatic over-expression of peroxisome proliferator activated receptor gamma2 in the ob/ob mouse model of non-insulin dependent diabetes mellitus. *Mol Cell Biochem* 224: 29–37.
63. Chao L, *et al.* (2000) Adipose tissue is required for the antidiabetic, but not for the hypolipidemic, effect of thiazolidinediones. *J Clin Invest* 106: 1221–1228.
64. Uno K, *et al.* (2006) Neuronal pathway from the liver modulates energy expenditure and systemic insulin sensitivity. *Science* 312: 1656–1659.
65. Lam TK, Schwartz GJ, Rossetti L (2005) Hypothalamic sensing of fatty acids. *Nat Neurosci* 8: 579–584.

[Autophagy 3:4, 405-407; July/August 2007]; ©2007 Landes Bioscience

Addendum

AMPK Mediates Autophagy During Myocardial Ischemia In Vivo

Hiromitsu Takagi[1]
Yutaka Matsui[1]
Shinichi Hirotani[1]
Hideyuki Sakoda[2]
Tomoichiro Asano[3]
Junichi Sadoshima[1,*]

[1]Cardiovascular Research Institute; Department of Cell Biology and Molecular Medicine; University of Medicine and Dentistry of New Jersey; New Jersey Medical School; Newark, New Jersey USA

[2]Department of Internal Medicine; Graduate School of Medicine; University of Tokyo; Tokyo, Japan

[3]Division of Molecular Medical Science; Programs for Biomedical Research; Hiroshima University; Hiroshima, Japan

*Correspondence to: Junichi Sadoshima; Cardiovascular Research Institute; University of Medicine and Dentistry of New Jersey; 185 South Orange Avenue; MSB G-609; Newark, New Jersey 07103 USA; Tel.: 973.972.8619; Fax: 973.972.7489; Email: Sadoshju@umdnj.edu

Original manuscript submitted: 04/10/07
Manuscript accepted: 04/13/07

Previously published online as an *Autophagy* E-publication:
http://www.landesbioscience.com/journals/autophagy/abstract.php?id=4281

KEY WORDS

ischemia, reperfusion, AMPK, autophagy, heart, beclin1

ACKNOWLEDGEMENTS

See page 406.

Addendum to:

Distinct Roles of Autophagy in the Heart During Ischemia and Reperfusion: Roles of AMP-Activated Protein Kinase and Beclin 1 in Mediating Autophagy

Y. Matsui, H. Takagi, X. Qu, M. Abdellatif, H. Sakoda, T. Asano, B. Levine and J. Sadoshima

Circ Res 2007; 100:914-22

ABSTRACT

We have recently shown that autophagy is induced by ischemia and reperfusion in the mouse heart in vivo. Ischemia stimulates autophagy through an AMP activated protein kinase (AMPK)-dependent mechanism, whereas reperfusion after ischemia stimulates autophagy through a Beclin 1-dependent, but AMPK-independent, mechanism. Autophagy plays distinct roles during ischemia and reperfusion: autophagy may be protective during ischemia, whereas it may be detrimental during reperfusion. We will discuss the role of AMPK in mediating autophagy during myocardial ischemia in vivo.

Autophagy is a major mechanism for degrading long-lived cytosolic proteins and is the only known pathway for degrading organelles.[1] Autolysosomal degradation of membrane lipids and proteins generates free fatty acids and amino acids, which can then be reused to maintain mitochondrial ATP production and ribosomal protein synthesis.[2] Autophagy is also activated in order to remove damaged organelles and stimulate phagocytic clearance of apoptotic cells.[3] Although the presence of autophagy has been shown in the heart, whether autophagy is salutary or detrimental for the heart remains unknown in vivo. We used a mouse model of myocardial ischemia/reperfusion in order to elucidate the functional roles of autophagy in pathologically relevant conditions in the heart.

In our model, myocardial ischemia (20 min) induced increases in autophagosome formation and, after reperfusion, the number of autophagosomes was further increased,[4] confirming the observation made by Decker more than 25 years ago.[5] In our mouse model of ischemia/reperfusion, the cellular ATP content decreases with ischemia and rapidly recovers after reperfusion, causing autophagosome formation to be stimulated serially, in two distinct conditions, namely energy-starved and energy-unstarved conditions.

AMP activated protein kinase (AMPK) belongs to a conserved family of protein kinases activated by ATP depletion and consequent AMP accumulation. AMPK plays an important role in regulating both fatty acid and glucose metabolism.[6] The yeast homolog, the sucrose nonfermenting protein 1 (Snf1)/Snf4 complex mediates autophagy during starvation, thereby mediating cell adaptation to a glucose-free environment.[7] In mammals, ATP depletion inhibits mammalian target of rapamycin (mTOR) through activation of AMPK and subsequent phosphorylation of tuberous sclerosis complex 2 (TSC2).[8] Since mTOR negatively regulates autophagy,[9] the AMPK-mTOR pathway has been proposed to be an important regulator of autophagy in response to starvation.[10,11] However, whether AMPK is involved in mediating autophagy has not been shown in vivo.

During myocardial ischemia, a rapid drop in intracellular ATP leads to the activation of AMPK. Autophagosomal formation, in response to myocardial ischemia, was decreased in dominant negative AMPK (DN-AMPK) overexpression mice, suggesting that endogenous AMPK plays an important role in mediating autophagy during myocardial ischemia.[4] During myocardial ischemia, the ATP content in the heart was lower, left ventricular (LV) end-diastolic pressure, an index of cardiac dysfunction, was higher, and release of creatine kinase and lactate dehydrogenase, an index of myocardial injury, was greater in the DN-AMPK mice compared with control mice.[12,13] Our new experiment shows that the size of myocardial infarction after extended ischemia (90 min) is greater in DN-AMPK mice than in wild type mice (Fig. 1). These results suggest that the induction of autophagy by AMPK may contribute to the preservation of ATP content as well as promotion of cell survival in the ischemic heart. It should be noted, however, that the activation of AMPK enhances ATP production through multiple mechanisms, including increases in glucose uptake, glycolysis, and fatty acid oxidation.[6] The contribution of autophagy to the overall actions of AMPK in the ischemic heart remains to be identified.

Cultured cardiac myocytes develop autophagy in response to glucose and amino acid deprivation.[4] Our preliminary results suggest that DN-AMPK inhibits autophagy that is induced by glucose deprivation, but not by amino acid deprivation, indicating that the involvement of AMPK in the induction of autophagy is stimulus-specific.

Activation of AMPK causes phosphorylation of TSC2, thereby leading to inhibition of mTOR.[8] In anoxic cardiac myocytes, however, activation of AMPK leads to an inhibition of protein synthesis through phosphorylation of eukaryotic elongation factor-2 (eEF2) rather than by the inhibition of mTOR.[14] In fact, despite significant activation of AMPK by ischemia, we were unable to observe a significant drop of p70 S6 kinase (p70S6K) phosphorylation by ischemia in vivo, suggesting that the activity of mTOR may not be significantly affected by myocardial ischemia in vivo.[4] Since eEF2 kinase, which phosphorylates eEF2, regulates autophagy,[15] ischemia-induced autophagy may be mediated through the AMPK-eEF2 kinase pathway rather than through the AMPK-induced inhibition of mTOR. AMPK may also stabilize p27 through phosphorylation, which in turn mediates autophagy.[16] In yeast, *SNF1* regulates two genes involved in autophagy, namely *ATG1* and *ATG13*, and autophagy critically regulates the maintenance of glycogen levels.[7] Since the AMPK α2 subunit contains a putative nuclear localization signal,[6] it is possible that DN-AMPK has direct effects upon the nuclear actions of AMPK, namely transcription of genes involved in autophagy.

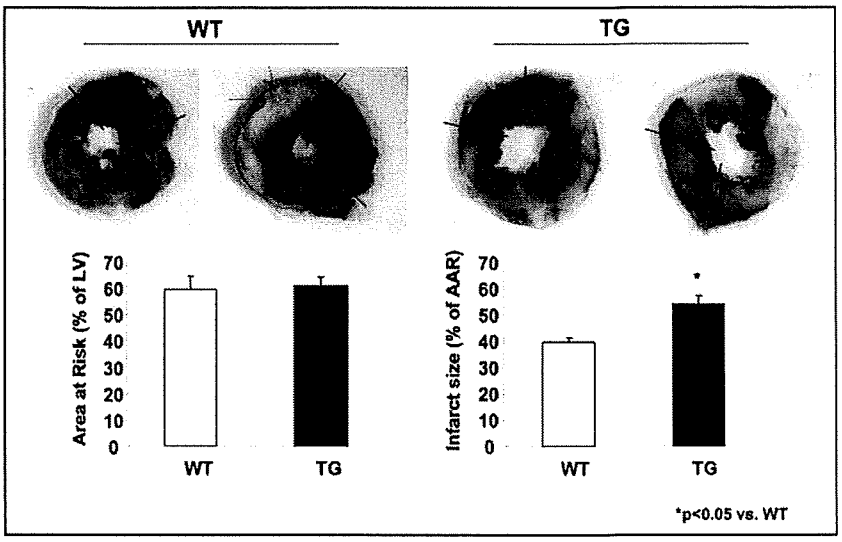

Figure 1. The effect of prolonged ischemia on the size of myocardial infarction in wild type (WT) (n = 3) and DN-AMPK (TG) (n = 3) mice. The mice were subjected to 90 min of ischemia. Area at risk (left) and the size of the myocardial infarction (right) were determined by Alcian Blue dye and TTC staining, respectively. The detailed method has been described previously.[4] Note that the size of the myocardial infarction was greater in DN-AMPK mice ($p < 0.05$) compared to WT.

Since AMPK is rapidly inactivated during reperfusion, it is unlikely that increases in autophagy during the reperfusion phase continue to be mediated by AMPK-dependent mechanisms.[4] In our model, autophagosomal formation during the reperfusion phase was critically mediated by Beclin 1-dependent mechanisms. Furthermore, both apoptosis and the size of the myocardial infarction during the reperfusion phase were reduced in *beclin 1*$^{+/-}$ mice, suggesting that autophagy during the reperfusion phase may be detrimental.[4] These results suggest that autophagy, in the presence or absence of energy starvation, could be mediated by distinct signaling mechanisms and have distinct functional significance (Fig. 2).

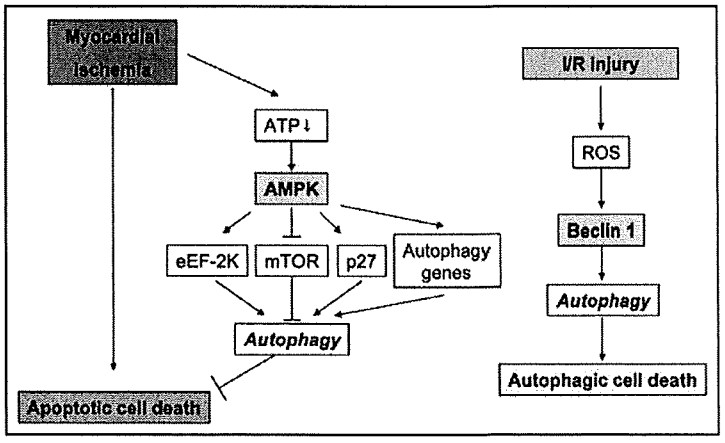

Figure 2. Schematic representation of a model of autophagy induced by myocardial ischemia or ischemia/reperfusion (I/R) injury in the heart. AMPK, AMP activated protein kinase; eEF-2K, eukaryotic elongation factor-2 kinase; mTOR, mammalian target of rapamycin; ROS, reactive oxygen species. Arrows (↓) indicate stimulatory effects, whereas antiparallel lines (⊥) represent inhibitory effects.

The question then arises should AMPK or autophagy be stimulated in situations such as chest pain due to myocardial ischemia? Based upon our previous studies,[4] stimulation of energy salvaging mechanisms during ischemia, including AMPK and autophagy, should be salutary. Controversy exists as to whether the stimulation of AMPK is beneficial for patients with myocardial ischemia, since the stimulation of fatty acid metabolism by AMPK could reduce glucose oxidation and make cardiac metabolism during ischemia less efficient.[17] Therefore, the therapeutic potential of AMPK during ischemia should be evaluated with caution. An alternative strategy to AMPK stimulation would be the direct stimulation of the autophagy machinery. In order to find a better strategy for cardioprotection based upon modulation of autophagy, however, the functional role of autophagy during myocardial ischemia/reperfusion should be defined using a method that regulates autophagy in a more specific and timely manner.

Acknowledgements

We thank Dr. Rong Tian (Brigham and Women's Hospital) for providing us with DN-AMPK mice, and Lauren Danridge for critical reading of the manuscript. This work was supported by U.S. Public Health Service Grants HL59139, HL67724, HL67727, HL69020, and HL73048 and by American Heart Association 0340123N.

References

1. Klionsky DJ, Ohsumi Y. Vacuolar import of proteins and organelles from the cytoplasm. Annu Rev Cell Dev Biol 1999; 15:1-32.
2. Lum JJ, DeBerardinis RJ, Thompson CB. Autophagy in metazoans: Cell survival in the land of plenty. Nat Rev Mol Cell Biol 2005; 6:439-48.
3. Qu X, Zou Z, Sun Q, Luby-Phelps K, Cheng P, Hogan RN, Gilpin C, Levine B. Autophagy gene-dependent clearance of apoptotic cells during embryonic development. Cell 2007; 128:931-46.
4. Matsui Y, Takagi H, Qu X, Abdellatif M, Sakoda H, Asano T, Levine B, Sadoshima J. Distinct roles of autophagy in the heart during ischemia and reperfusion: Roles of AMP-activated protein kinase and Beclin 1 in mediating autophagy. Circ Res 2007; 100:914-22.
5. Decker RS, Wildenthal K. Lysosomal alterations in hypoxic and reoxygenated hearts. I. Ultrastructural and cytochemical changes. Am J Pathol 1980; 98:425-44.
6. Arad M, Seidman CE, Seidman JG. AMP-activated protein kinase in the heart: Role during health and disease. Circ Res 2007; 100:474-88.
7. Wang Z, Wilson WA, Fujino MA, Roach PJ. Antagonistic controls of autophagy and glycogen accumulation by Snf1p, the yeast homolog of AMP-activated protein kinase, and the cyclin-dependent kinase Pho85p. Mol Cell Biol 2001; 21:5742-52.
8. Inoki K, Corradetti MN, Guan KL. Dysregulation of the TSC-mTOR pathway in human disease. Nat Genet 2005; 37:19-24.
9. Noda T, Ohsumi Y. Tor, a phosphatidylinositol kinase homologue, controls autophagy in yeast. J Biol Chem 1998; 273:3963-6.
10. Meley D, Bauvy C, Houben-Weerts JH, Dubbelhuis PF, Helmond MT, Codogno P, Meijer AJ. AMP-activated protein kinase and the regulation of autophagic proteolysis. J Biol Chem 2006; 281:34870-9.
11. Samari HR, Seglen PO. Inhibition of hepatocytic autophagy by adenosine, aminoimidazole-4-carboxamide riboside, and N6-mercaptopurine riboside: Evidence for involvement of amp-activated protein kinase. J Biol Chem 1998; 273:23758-63.
12. Xing Y, Musi N, Fujii N, Zou L, Luptak I, Hirshman MF, Goodyear LJ, Tian R. Glucose metabolism and energy homeostasis in mouse hearts overexpressing dominant negative $\alpha 2$ subunit of AMP-activated protein kinase. J Biol Chem 2003; 278:28372-7.
13. Russell IIIrd RR, Li J, Coven DL, Pypaert M, Zechner C, Palmeri M, Giordano FJ, Mu J, Birnbaum MJ, Young LH. AMP-activated protein kinase mediates ischemic glucose uptake and prevents postischemic cardiac dysfunction, apoptosis, and injury. J Clin Invest 2004; 114:495-503.
14. Horman S, Beauloye C, Vertommen D, Vanoverschelde JL, Hue L, Rider MH. Myocardial ischemia and increased heart work modulate the phosphorylation state of eukaryotic elongation factor-2. J Biol Chem 2003; 278:41970-6.
15. Wu H, Yang JM, Jin S, Zhang H, Hait WN. Elongation factor-2 kinase regulates autophagy in human glioblastoma cells. Cancer Res 2006; 66:3015-23.
16. Liang J, Shao SH, Xu ZX, Hennessy B, Ding Z, Larrea M, Kondo S, Dumont DJ, Gutterman JU, Walker CL, Slingerland JM, Mills GB. The energy sensing LKB1-AMPK pathway regulates p27(kip1) phosphorylation mediating the decision to enter autophagy or apoptosis. Nat Cell Biol 2007; 9:218-24.
17. Dyck JR, Lopaschuk GD. AMPK alterations in cardiac physiology and pathology: Enemy or ally? J Physiol 2006; 574:95-112.

MOLECULAR AND CELLULAR BIOLOGY, Apr. 2007, p. 2548–2561 Vol. 27, No. 7
0270-7306/07/$08.00+0 doi:10.1128/MCB.00992-06

Calpain 6 Is Involved in Microtubule Stabilization and Cytoskeletal Organization▽†

Kazuo Tonami,[1] Yukiko Kurihara,[1] Hiroyuki Aburatani,[2] Yasunobu Uchijima,[1] Tomoichiro Asano,[3] and Hiroki Kurihara[1]*

Department of Physiological Chemistry and Metabolism, Graduate School of Medicine, The University of Tokyo, 7-3-1 Hongo, Bunkyo-ku, Tokyo 113-0033, Japan[1]; Genome Science Division, Research Center for Advanced Science and Technology, The University of Tokyo, 4-6-1 Komaba, Meguro-ku, Tokyo 153-8904, Japan[2]; and Department of Biomedical Chemistry, Hiroshima University Graduate School of Biomedical Sciences, Kasumi 1-2-3, Hiroshima 734-8551, Japan[3]

Received 5 June 2006/Returned for modification 11 July 2006/Accepted 21 December 2006

The calpains are a family of Ca^{2+}-dependent cysteine proteases implicated in various biological processes. In this family, calpain 6 (Capn6) is unique in that it lacks the active-site cysteine residues requisite for protease activity. During the search for genes downstream of the endothelin 1 (ET-1) signaling in pharyngeal-arch development, we identified Capn6. After confirming that the expression of Capn6 in pharyngeal arches is downregulated in ET-1-null embryos by in situ hybridization, we investigated its function. In Capn6-transfected cells, cytokinesis was retarded and was often aborted to yield multinucleated cells. Capn6 overexpression also caused the formation of microtubule bundles rich in acetylated α-tubulin and resistant to the depolymerizing activity of nocodazole. Green fluorescent protein-Capn6 overexpression, immunostaining for endogenous Capn6, and biochemical analysis demonstrated interaction between Capn6 and microtubules, which appeared to be mainly mediated by domain III. Furthermore, RNA interference-mediated Capn6 inactivation caused microtubule instability with a loss of acetylated α-tubulin and induced actin reorganization, resulting in lamellipodium formation with membrane ruffling. Taken together, these results indicate that Capn6 is a microtubule-stabilizing protein expressed in embryonic tissues that may be involved in the regulation of microtubule dynamics and cytoskeletal organization.

The calpains are a family of intracellular cysteine proteases whose activities are highly dependent on Ca^{2+} ions (9, 11, 16, 35, 36, 38). Fourteen members of the calpain family are known in mammals, whereas a large number of molecules with structural similarity have been reported to constitute a superfamily beyond species. Calpain 1 (Capn1) (μ-calpain) and Capn2 (m-calpain) are the representative members most extensively studied. They heterodimerize with a small regulatory subunit, Capn4. These "classical" calpains are ubiquitously expressed and are implicated in various cellular functions, such as migration, apoptosis, cell growth, and cell cycle progression. p94/Capn3 is a skeletal-muscle-specific calpain whose loss-of-function mutation causes limb girdle muscular dystrophy type 2A (11, 16, 35). Capn10 has been identified as a molecule associated with an increased risk for type 2 diabetes (11, 16). To date, many proteins have been proposed as candidates for their enzymatic substrates, although the physiologically relevant substrates remain largely unknown (11).

Many large-molecule calpains share a common four-domain structure consisting of domains I to IV (9, 11, 16, 35, 36, 38). Domain II is divided into subdomains IIa and IIb, which generate a substrate-binding cleft between them. The crystal structure of Capn2 has revealed that the cysteine residue in subdomain IIa and the histidine and asparagine residues in subdomain IIb form a catalytic triad (13, 30, 37). Domain III is related to the C2 domain, a Ca^{2+}- and phospholipid-binding module (33). Domain IV is characterized by the presence of multiple EF-hand motifs in Capn1, -2, -3, -8, -9, -11, and -12, whereas other calpains have distinct structures in their C-terminal regions. In Capn5 and Capn6, the C-terminal structure is defined as the T domain, based on homology to *Caenorhabditis elegans* TRA-3, a nematode sex determination factor (35), but the function of this domain is unclear.

In the calpain family, Capn6 is unique in that it lacks the active-site catalytic cysteine residue and may not be a proteolytic enzyme (4). *Capn6* is located on the X chromosome and is expressed during embryogenesis (4, 5, 26). In particular, the mandibular arch, somite and developing skeletal muscle, heart, epithelial border of the fourth ventricle, lobar bronchi, capsule of the lung and kidney, and chorionic plate of the placenta highly express *Capn6* from the mid- to late-embryonic stages (5). In contrast, *Capn6* expression appears to be downregulated after birth (5). These findings led us to postulate some important roles for Capn6 in embryonic development; however, no functional characterization has been reported for Capn6.

Various developmental processes are controlled by genetic hierarchies involved in interactions among different cell populations. In mandibular-arch development, endothelin 1 (ET-1), a 21-amino-acid peptide originally identified as a vascular-endothelium-derived vasoconstrictor (25, 42), has emerged as a regulator of the dorsoventral axis patterning through the

* Corresponding author. Mailing address: Department of Physiological Chemistry and Metabolism, Graduate School of Medicine, University of Tokyo, 7-3-1 Hongo, Bunkyo-ku, Tokyo 113-0033, Japan. Phone: 81-3-5841-3498. Fax: 81-3-5684-4958. E-mail: kuri-tky@umin.ac.jp.

† Supplemental material for this article may be found at http://mcb.asm.org/.

▽ Published ahead of print on 8 January 2007.

induction of *Dlx5* and *Dlx6*, homeobox genes belonging to the vertebrate *Distal-less* homologues (2, 7, 19, 21, 22, 29). However, key molecules downstream of this genetic hierarchy controlling pharyngeal-arch development remain largely unknown. While exploring such downstream genes by microarray analysis, we encountered Capn6 as a candidate molecule. Its expression pattern in the pharyngeal arch and unique molecular form among the calpain family members inclined us to pursue its role in pharyngeal-arch development. To start with, we decided to unveil the molecular function of this molecule. Here, we demonstrate that Capn6 is a microtubule-stabilizing protein. Capn6 overexpression causes a failure of cytokinesis, leading to the formation of multinucleated cells. Immunocytochemical and biochemical analyses revealed the association of Capn6 with microtubules, which appeared to be mediated by domain III. In addition, RNA interference (RNAi)-mediated Capn6 inactivation resulted in a loss of stable microtubules and induced actin reorganization, resulting in lamellipodium formation with membrane ruffling. These results suggest that Capn6 may be involved in the regulation of microtubule stability and actin organization. During pharyngeal-arch development, Capn6 may act as a downstream molecule of ET-1 signaling through its effect on cytoskeletal organization.

MATERIALS AND METHODS

Microarray analysis. Total RNA was extracted from excised embryonic day 10.5 (E10.5) mandibular arches of *ET-1*$^{-/-}$ embryos with ISOGEN (Nippon Gene). Each cDNA sample was synthesized from the total RNA with a Superscript kit (Clontech) and was hybridized to a GeneChip array containing about 12,500 mouse genes. The hybridized arrays were scanned and analyzed with the Affymetrix GeneChip System. The relative abundance of each gene was estimated from the average difference of intensities. Change was calculated by taking the difference in average differences between the *ET-1*$^{+/\pm}$ (wild-type and homozygous) and *ET-1*$^{-/-}$ samples. The score of increase, decrease, or no change of expression for individual genes was defined on the basis of ranking the difference calls from three intergroup comparisons (3 × 3) as follows: no change = 0, marginal increase/decrease = 1/−1, and increase/decrease = 2/−2. The final rank was assigned by summing up the nine values corresponding to the difference calls, and the values varied from −18 to 18. The cutoff value for the final determination of increase/decrease was set as 9/−9.

Plasmids. The 3′ untranslated region of *Capn6* was amplified by reverse transcription (RT)-PCR of cDNA samples from E10.5 mandibular arches and subcloned into the pCRII TOPO vector (Invitrogen) for the generation of antisense riboprobes. For the expression of green fluorescent protein (GFP) fusion protein, the *Capn6* open reading frame and its PCR-amplified deletion mutants were subcloned in frame into the pEGFP-C2 expression vector (Clontech). Wild-type Capn6 expression vectors were constructed by cutting out the GFP gene from pEGFP-Capn6 expression plasmids. For the glutathione *S*-transferase (GST) fusion protein, *Capn6* and its deletion mutants were subcloned in frame into the PGEX-4T-1 vector (Amersham). All of the constructs were verified by sequencing.

Whole-mount in situ hybridization. The *ET-1*$^{-/-}$ mouse was described previously (20). Embryos were harvested at E10.5 and fixed in 4% paraformaldehyde–phosphate-buffered saline (PBS). Whole-mount in situ hybridization was performed as described by Wilkinson using a digoxigenin-labeled *Capn6* riboprobe (41).

Generation of Capn6 antibody. Polyclonal antibody against mouse Capn6 was generated at Transgenic Inc. by injecting a rabbit with a keyhole limpet hemocyanin-conjugated synthetic oligopeptides corresponding to the C-terminal domain of Capn6 (amino acids 605 to 617). The bleeds were affinity purified using Affi-Gel 10 gel (Bio-Rad) coupled with the oligopeptides.

Cell culture and transfection. NIH 3T3, HeLa, and HEK 293T cells were cultured in Dulbecco's modified Eagle's medium containing 10% fetal calf serum and antibiotics at 37°C in 5% CO_2. For transfection, cells were grown to 50 to 90% confluence and were treated with a mixture of plasmid DNA and LipofectAMINE PLUS or LipofectAMINE 2000 reagent (Invitrogen). After 2 to 3 h of incubation, the cells were refed with medium containing fetal calf serum and were allowed to recover for 24 to 48 h. Cells transfected with plasmids encoding GFP derivatives were observed by fluorescence microscopy. For stable transformants of GFP-tubulin, linearized pEGFP-Tub vector (BD Biosciences) was transfected into NIH 3T3 cells and selected with G418. Several independent clones were picked up, and expression was confirmed by fluorescence microscopy and Western blotting.

Immunofluorescence microscopy. Cells were washed with preincubated general tubulin buffer (GTB) {80 mM PIPES [piperazine-*N*,*N*′-bis(2-ethanesulfonic acid)], pH 7, 1 mM $MgCl_2$, 1 mM EGTA} at 37°C, fixed with 4% paraformaldehyde in GTB, permeabilized with 0.2% Triton X-100 in GTB, and washed with GTB at room temperature. After being blocked with 5% skim milk in GTB, the cells were incubated with primary antibodies as follows; the rabbit polyclonal anti-Capn6 antibody, rabbit polyclonal anti-GFP antibody (MBL), and mouse monoclonal anti-α-tubulin and anti-acetylated α-tubulin antibodies (Sigma). Then, the cells were washed and stained with the secondary antibodies (fluorescein isothiocyanate- or rhodamine-conjugated donkey anti-mouse or rabbit immunoglobulin G; Jackson Immunoresearch). For actin staining, 2.5 units/ml rhodamine-phalloidin (Invitrogen) was added to the reaction buffer containing fluorescein isothiocyanate-conjugated secondary antibody. The cells were viewed using a fluorescence microscope (Nikon TE300) or a confocal microscope (Nikon D-ECLIPSE C1). Three-dimensional views (see Fig. 3F and G) were produced from 28 images in a two-dimensional Z stack spanning about 0.15 μm of the center of a single cell using EZ-C1 2.30 (Nikon) software.

Time-lapse video microscopy. Cells were grown on 35-mm culture dishes set in a control chamber maintained at 5% CO_2-95% air at 37°C. Cell images were obtained from 12 to 16 h after transfection at 5-min (for GFP-Capn6 overexpression experiments) or 1-min (for RNAi experiments) intervals on a TE300 microscope (Nikon) using a 20× Nikon objective lens (numerical aperture, 0.45) and an ORCA 100 cooled charge-coupled-device camera (Hamamatsu) and analyzed by AquaCosmos imaging software (Hamamatsu).

Western blotting. For whole-cell lysate preparation, cells were solubilized in PBS containing 1% Triton X-100, 0.1% sodium deoxycholate, 0.02% sodium dodecyl sulfate (SDS), 1 mM phenylmethylsulfonyl fluoride, 0.5 mM vanadate, and protease inhibitor cocktail (Sigma). For crude fractionation, cells were suspended in 80 mM PIPES, pH 7.0, 0.1% NP-40, 1 mM $MgCl_2$, 1 mM EGTA, 1 mM phenylmethylsulfonyl fluoride, 0.5 mM vanadate, and protease inhibitor cocktail (Sigma). After incubation for 15 min on ice, the suspension was passed through a 27-gauge syringe needle and centrifuged at 800 × *g* for 5 min at 4°C. The supernatant was saved as the soluble fraction. The pellet was resuspended in PBS containing 1% Triton X-100 and protease inhibitors, sonicated for 10 s, and subjected to protein analysis. The protein concentration was determined using a bicinchoninic acid protein assay kit (Pierce), and equal volumes of proteins were separated by 7.5% SDS-polyacrylamide gel electrophoresis (PAGE) and then electrotransferred to a polyvinylidene difluoride (PVDF) membrane. After being blocked with 5% skim milk in 0.1% Tween 20 in Tris-buffered saline, pH 7.6, the blots were probed with primary antibodies as follows: rabbit polyclonal anti-Capn6 antibody; rabbit polyclonal anti-GFP antibody (MBL); rabbit polyclonal anti-μ-calpain (Capn1) antibody (Sigma); mouse monoclonal anti-α-tubulin, anti-acetylated α-tubulin, and anti-β-actin antibodies (Sigma); and goat polyclonal anti-MAP4 antibody (Santa Cruz). The membranes were then washed with 0.1% Tween 20 in Tris-buffered saline, pH 7.6, and incubated with peroxidase-conjugated anti-rabbit, anti-mouse, or anti-goat immunoglobulin G (DAKO). The signals were detected using the ECL chemiluminescence detection system (Amersham Bioscience).

Microtubule cosedimentation assay. Cells were lysed in 80 mM PIPES, pH 7.0, 1% Triton X-100, 1 mM $MgCl_2$, 1 mM EGTA, 1 mM phenylmethylsulfonyl fluoride, 0.5 mM vanadate, and protease inhibitor cocktail (Sigma) by passing them through a 30-gauge syringe needle. After incubation on ice for 30 min to depolymerize the microtubules, the lysate was centrifuged at 20,000 × g for 80 min at 4°C to remove cellular debris. The supernatant was divided into two tubes, and 20 μM paclitaxel (Taxol) or vehicle (dimethyl sulfoxide [DMSO]) was added to each sample. After incubation for 30 min at 37°C, the reaction mixture was centrifuged at 20,000 × *g* for 40 min at room temperature. The resultant pellets were resuspended in lysis buffer, separated by 7.5% SDS-PAGE, and subjected to Western blotting analysis with whole lysate and supernatants.

Microtubule binding assay on filter paper. GST-fused full-length Capn6 protein was tested for microtubule binding on filter paper according to the method previously described by Nakaseko et al. (28). Briefly, GST-Capn6 fusion proteins were purified from bacterial lysates by using glutathione beads and subjected to SDS-PAGE. Then, the proteins were transferred to a PVDF filter and incubated in 100 mM PIPES, pH 6.9, 2 mM EGTA, 1 mM $MgSO_4$, 0.1% Tween 20, and 5% skim milk, followed by an additional incubation with paclitaxel-stabilized bovine brain microtubules (50 μg/ml; Cytoskeleton Inc.) in the same buffer. The filter

was then washed and immunoblotted with anti-tubulin antibody. Purified MAP2 (Cytoskeleton Inc.) served as a positive control.

GST pull-down assay. For cell lysate preparation, NIH 3T3 cells were solubilized in pull-down buffer (20 mM Tris-HCl, pH 7.6, 1% Triton X-100, 0.25% sodium deoxycholate, 0.25 M NaCl) containing 1 mM phenylmethylsulfonyl fluoride, 0.5 mM vanadate, and protease inhibitor cocktail (Sigma). The solubilized cell lysates were frozen and thawed twice and sonicated 25 times for 10 s each time. Unbroken cells and cellular debris were removed by centrifugation at 20,000 × *g* at 4°C for 10 min. After incubation on ice for 15 min, the lysates were incubated with 20 μM paclitaxel and 1 mM GTP at 37°C for 30 min to stabilize the microtubules. Then, GST fusion proteins bound to the beads were mixed with lysates and incubated at 4°C for 6 h. The beads were washed three times with pull-down buffer containing protease inhibitors, and the bound proteins were eluted by adding 2.5× sample buffer and then boiled for 5 min. These samples were subjected to 10% (vol/vol) SDS-PAGE, and proteins were detected by Western blotting with anti-α-tubulin or anti-acetylated α-tubulin antibodies. The amounts of GFP fusion proteins were grossly estimated by Ponceau staining.

siRNA experiments. Two different stealth small interfering RNA (siRNA) duplexes designated no. 1298 and 1715, which targeted nucleotides 1298 to 1322 and 1715 to 1739 of the mouse Capn6 mRNA sequence, respectively, and control siRNA containing the same nucleotides as no. 1298 but with scrambled sequence were synthesized by Invitrogen. The sense sequences of 1298, 1715, and control siRNAs were 5′-GGUUCCGUCUUCACCAUCUGUAUAU-3′, 5′-GGACCA CUGACAUUCCUAUUAUCAU-3′, and 5′-GGUUGCUUCCACUACGUCA UUCUAU-3′, respectively. The siRNAs were transfected into NIH 3T3 cells using OligofectAMINE (Invitrogen) according to the manufacturer's protocol. In some experiments, GFP-tubulin-expressing NIH 3T3 cells were used. The efficiency of gene knockdown was evaluated by RT-PCR with primers specific for the mouse *Capn6* mRNA (sense, 5′-GAATGTGGACATCCTACATG-3′; antisense, 5′-GCTGTCCTATTACTGAATAG-3′) and Western blotting. Expression of glyceraldehyde-3-phosphate dehydrogenase (GAPDH) and β-actin served as internal controls for RT-PCR and Western blotting, respectively.

RESULTS

Endothelin-1-dependent *Capn6* expression in pharyngeal-arch development. To explore target genes downstream of the ET-1 signaling involved in pharyngeal-arch development, we performed oligonucleotide microarray analysis on E10.5 *ET-1*$^{-/-}$ and *ET-1*$^{+/\pm}$ mandibular arches to identify genes downstream of the ET-1 signaling in mandibular-arch development. Among 132 genes with decreases in the E10.5 *ET-1*$^{-/-}$ mandibular arch in comparison to the *ET-1*$^{+/\pm}$ control (data not shown), *Capn6* was found to be decreased by ~2.8-fold.

To confirm the downregulation of *Capn6* in the *ET-1*$^{-/-}$ mandibular arch, we performed whole-mount in situ hybridization. *Capn6* expression was detected in the mandibular arch, heart, limb buds, and somites during embryogenesis, suggesting its tissue-specific role during embryonic development (Fig. 1A and C). In the *ET-1*$^{-/-}$ mutant, *Capn6* expression was downregulated in the mandibular-arch mesenchyme, whereas its expression in the most dorsal mandibular epithelium was preserved (Fig. 1B and D). *Capn6* expression in other regions was not affected in the *ET-1*$^{-/-}$ mutant (Fig. 1B).

Capn6 induces multinucleation by interfering with cytokinesis. To characterize the function of Capn6, we fused Capn6 to GFP and overexpressed it in HeLa cells. Among cells transfected with GFP-Capn6, ~20% became bi- or trinucleated 48 h after transfection, whereas only ~3% of control GFP-transfected cells became multinucleated (Fig. 2A to C). Overexpression of wild-type Capn6 also induced multinucleation with comparable frequency (data not shown), suggesting that this effect was not due to GFP fusion. When HEK 293T cells were transfected, almost all Capn6-transfected cells became multinucleated within 7 to 10 days, sometimes with ~10 nuclei (data not shown).

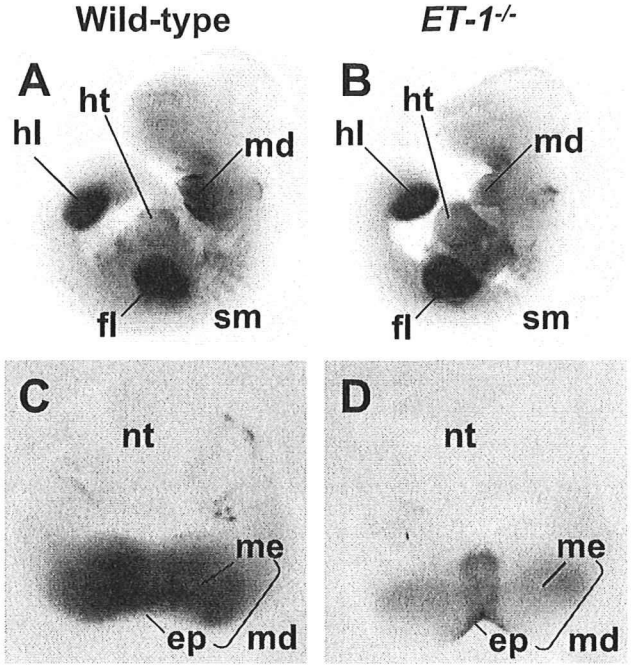

FIG. 1. Expression of *Capn6* in mouse embryos. Whole-mount in situ hybridization was performed on E10.5 wild-type (A and C) and *ET-1*$^{-/-}$ (B and D) embryos using the *Capn6* probe. Whole bodies (A and B) and excised mandibular arches (C and D) are shown. *Capn6* is normally expressed in the mandibular arches, heart, and limb buds. In the *ET-1*$^{-/-}$ mutant, the expression of *Capn6* in the mandibular arches is specifically downregulated, whereas *Capn6* expression in other regions is not affected. ep, epithelium; fl, forelimb bud; hl, hindlimb bud; ht, heart; md, mandibular arch; me, mesenchyme; nt, neural tube; sm, somites.

To explore the cause of the multinucleation induced by Capn6, we followed the fate of Capn6-transfected HeLa cells under time-lapse video microscopy. In all the control GFP-expressing cells examined (n = 13), the cleavage furrow started to ingress within 5 min and daughter cells flattened out within 30 min after the onset of anaphase (Fig. 2D; see Video S1 in the supplemental material). Thereafter, the cytoplasmic bridge disappeared within 90 min (Fig. 2D). Among GFP-Capn6-expressing mitotic cells examined (n = 15), 12 cells were able to complete cell division eventually, but the progression of furrow ingression was obviously retarded in 10 of the 12 cells (Fig. 2E; see Video S2 in the supplemental material). Eight of 12 daughter pairs retained a peanut-shaped morphology at 90 min after anaphase onset, whereas 2 daughter pairs were still tethered to each other with the cytoplasmic bridge beyond 90 min. The other two cells, in which GFP signals were relatively low, showed no apparent retardation of cytokinesis (data not shown). In 3 of 15 cells examined, GFP-Capn6 overexpression caused regression of the cleavage furrow at various time points to yield binucleated cells (Fig. 2F; see Video S3 in the supplemental material). All the Capn6-overexpressing cells commenced mitosis and cytokinesis apparently normally, with the cleavage furrow being appropriately positioned (Fig. 2E and F; see Video S4 in the supplemental material) indicating that Capn6 does not affect the onset of anaphase and cleavage furrow formation. Instead, Capn6 overexpression can disrupt

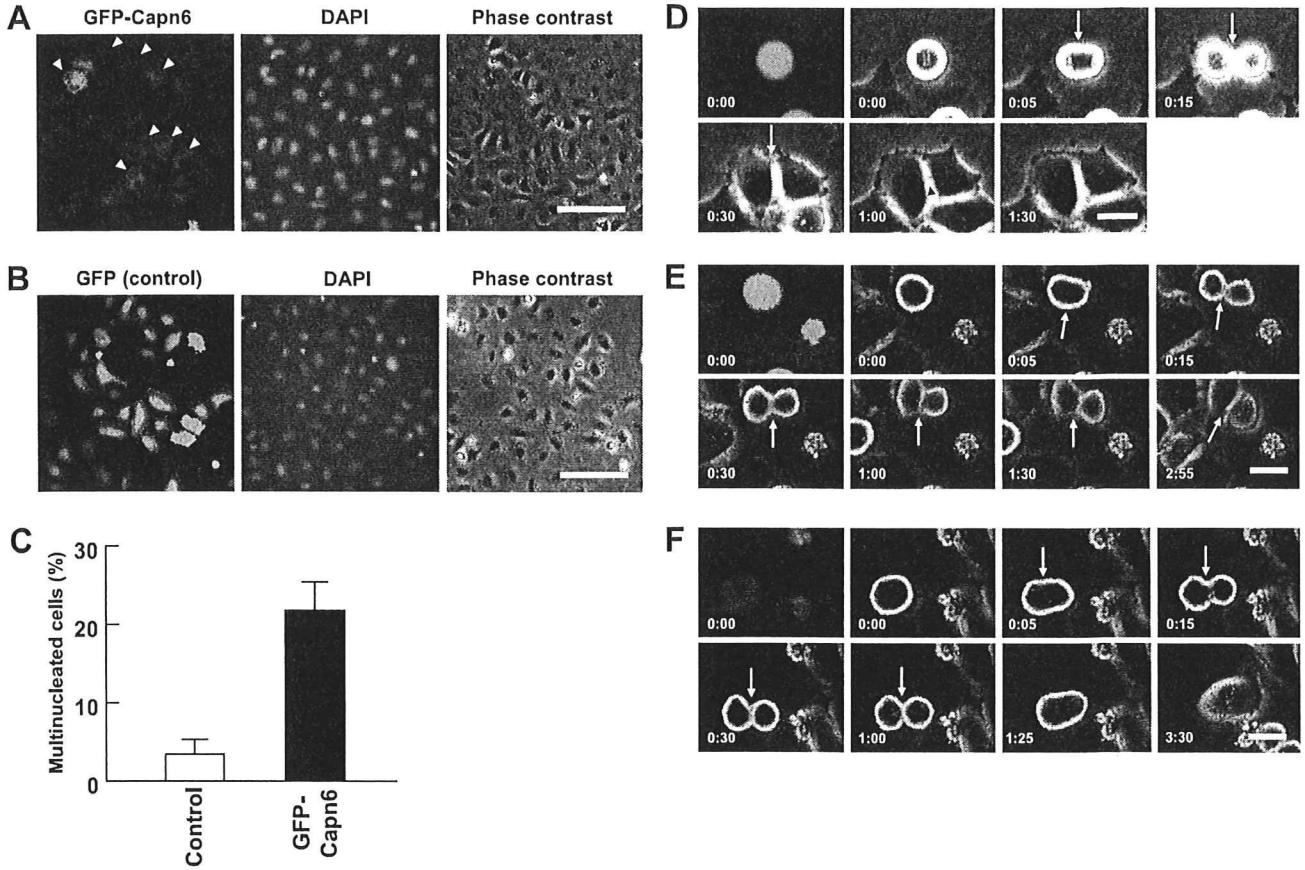

FIG. 2. GFP-Capn6 overexpression impairs cytokinesis and causes the formation of multinucleated cells. (A and B) Multinucleation of HeLa cells by GFP-Capn6 overexpression. Many GFP-Capn6-transfected cells become binucleated (arrowheads) 48 h after transfection (A), whereas most control GFP-transfected cells are mononucleated (B). The scale bars indicate 100 μm. (C) Comparison of multinucleated-cell numbers between control and GFP-Capn6-transfected cells 48 h after transfection. The data represent the mean and standard deviation of four independent experiments. (D to F) Representative images from time-lapse recordings of HeLa cells transiently expressing GFP (D) or GFP-Capn6 (E and F). (D) In control GFP-expressing cells, the cleavage furrow (arrows) started to ingress within 5 min and daughter cells flattened out within 30 min after the onset of anaphase. The cytoplasmic bridge (arrowhead) disappeared within 90 min. (E) In many GFP-Capn6-expressing cells, furrow formation started normally, but its progression was retarded. (F) In some cases, GFP-Capn6 overexpression caused regression of the cleavage furrow to yield binucleated cells. Time is in h/min after anaphase onset (0:00 time point). The scale bars indicate 20 μm.

the progression and completion of cytokinesis, often leading to the formation of multinucleated cells.

GFP-Capn6 colocalizes to and stabilizes the microtubule network. The failure of cytokinesis in Capn6-overexpressing cells led us to speculate that Capn6 may associate with cytoskeletal proteins involved in cytokinesis. To investigate this possibility, we examined the intracellular distribution of GFP-Capn6. In contrast to the diffuse distribution of control GFP protein throughout the cytoplasm and nucleus (Fig. 3A and F and 4A), GFP-Capn6 was mainly distributed in the perinuclear region in HeLa cells (Fig. 3B and G) or in a fascicular pattern in NIH 3T3 cells (Fig. 4C). Costaining with anti-tubulin antibody revealed that these distributions largely overlapped with thick microtubule bundles, whose formation appeared to be facilitated by Capn6 overexpression (Fig. 3B and 4C).

During mitosis, GFP-Capn6 was distributed in association with the mitotic spindle (Fig. 3C). At telophase, GFP-Capn6 was most intensely colocalized to microtubules in the central spindle (Fig. 3D). This colocalization was sustained in the midbody toward the end of cytokinesis, although a large portion of the GFP signals appeared to be distributed throughout the cytoplasm (Fig. 3E).

To determine the nature of microtubule bundles induced by Capn6 overexpression, we examined the level of tubulin acetylation, a posttranslational modification characteristic of stable microtubules (32). Immunostaining with specific antibody revealed that microtubules in GFP-Capn6-overexpressing cells contained high levels of acetylated α-tubulin (Fig. 3G), whereas cells expressing GFP alone did not (Fig. 3F). In particular, the distribution of acetylated α-tubulin corresponded to Capn6-induced microtubule bundles in the perinuclear region in many transfected HeLa cells (Fig. 3G).

To confirm the increase in acetylated α-tubulin by Capn6, immunoblotting was performed on GFP- and GFP-Capn6-transfected HeLa cells. Acetylated α-tubulin levels were increased in GFP-Capn6-transfected cells compared to GFP-transfected cells, whereas total α-tubulin levels were not increased (Fig. 3H). Paclitaxel, a microtubule-stabilizing agent,

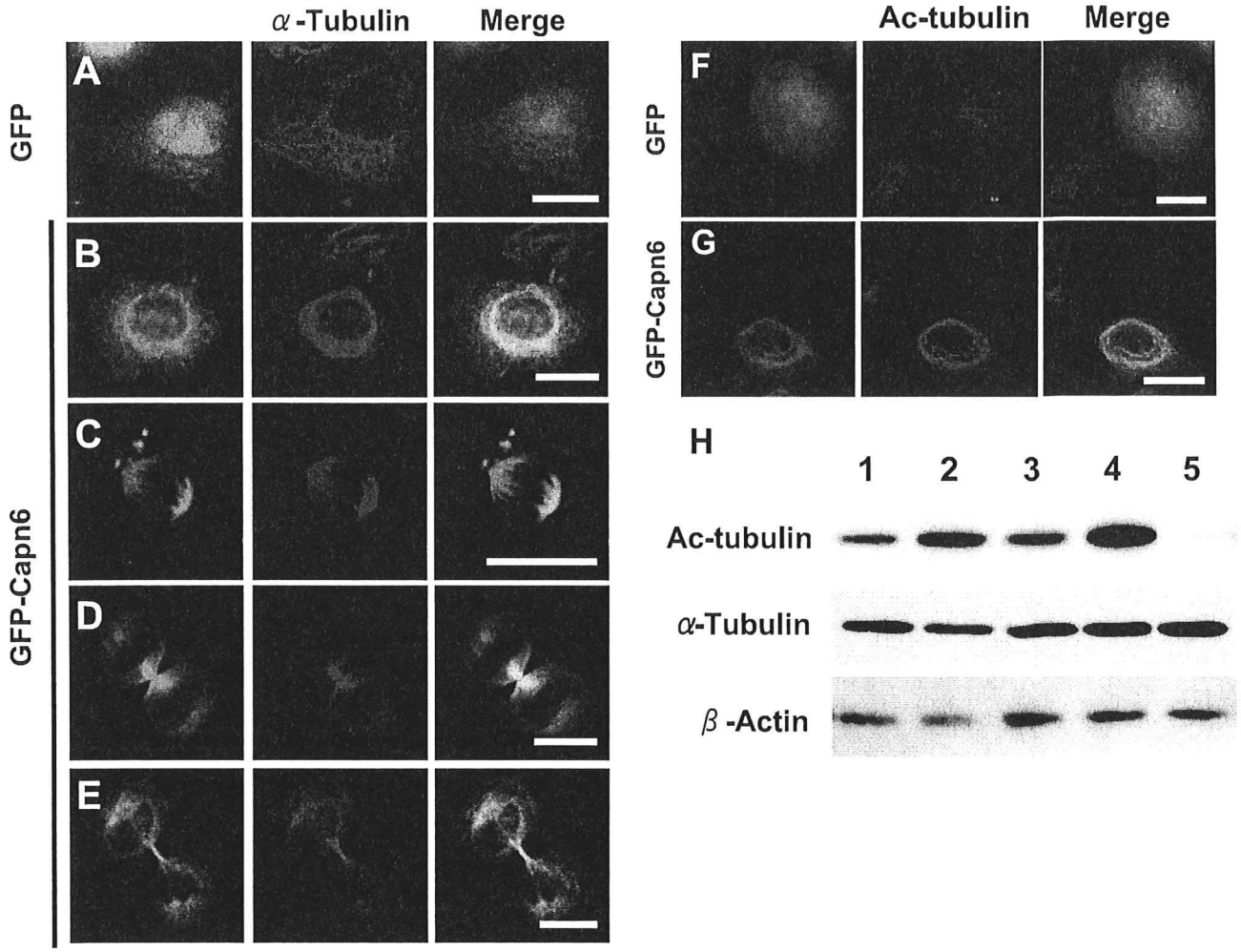

FIG. 3. Subcellular localization of GFP-Capn6 in HeLa cells at various stages of the cell cycle and its stabilizing effect on microtubules. (A to G) Cells were transfected with expression plasmids containing GFP (A and F) or GFP-Capn6 (B to E and G). After 24 h, the cells were stained with the anti-GFP antibody and anti-α-tubulin (A to E) or anti-acetylated α-tubulin (F and G) antibody. Notably, perinuclear microtubule bundling was observed in GFP-Capn6-transfected cells at interphase (B). During mitosis, GFP-Capn6 was distributed in association with the mitotic spindle (C). At telophase, GFP-Capn6 colocalized to the central spindle (D). At the late stage of cytokinesis, GFP-Capn6 colocalized to the midbody, whereas a large portion of the GFP signals were distributed throughout the cytoplasm (E). Three-dimensional Z-stack images show that the acetylated α-tubulin contents (Ac-tubulin), especially in the perinuclear region, were increased in GFP-Capn6-transfected cells (F and G). The scale bars indicate 20 μm. (H) HeLa cells were transfected with GFP (lane 1) or GFP-Capn6 (lane 2), lysed 16 h after transfection, and blotted with anti-acetylated α-tubulin, anti-α-tubulin, and anti-β-actin antibodies. HeLa cells were treated with DMSO (lane 3), 500 nM paclitaxel (lane 4), or 5 μM nocodazole (lane 5) for 1 h and blotted similarly to serve as controls for changes in acetylated α-tubulin levels. Acetylated-α-tubulin levels were increased in GFP-Capn6-transfected cells compared with GFP-transfected cells, whereas total α-tubulin levels were not increased. Blotting for β-actin served as an internal control. Similar results were obtained in three independent experiments. Representative data are shown.

and nocodazole, a microtubule-disrupting agent, induced increase and decrease in acetylated α-tubulin levels, respectively (Fig. 3H), indicating that the increase in acetylated α-tubulin in GFP-Capn6-transfected cells may reflect increased stability of microtubules.

In addition, the stability of microtubule bundles was tested by treatment with low-dose nocodazole. In cells expressing GFP alone, the microtubule network was largely disrupted by 500 nM nocodazole (Fig. 4A and B). In contrast, microtubule bundles induced by GFP-Capn6 were resistant to 500 nM nocodazole (Fig. 4C and D). These results indicate that Capn6-induced microtubule bundling is likely due to increased stability of microtubules.

Capn6 is a calpain family member that lacks active-site cysteine and histidine residues critical for proteolysis. It is therefore unlikely that the microtubule-stabilizing effect of Capn6 is mediated by protease activity common to other calpains. Indeed, the calpain inhibitors E-64 and Z-LLal did not inhibit the Capn6-induced formation of microtubule bundles (data not shown).

Endogenous Capn6 associates with microtubules. To further characterize the nature of Capn6, we raised a polyclonal

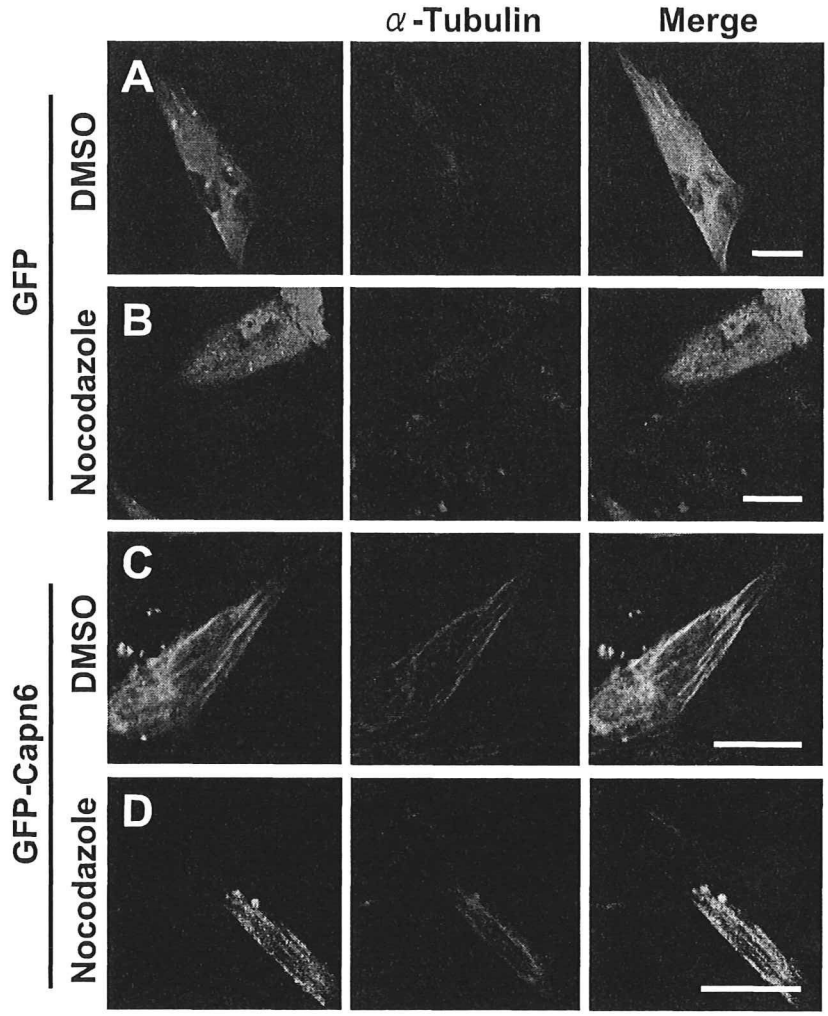

FIG. 4. GFP-Capn6 colocalizes to the microtubule network and induces microtubule bundling. NIH 3T3 cells were transfected with expression plasmids containing GFP (A and B) or GFP-Capn6 (C and D). After 16 h, the cells were treated with DMSO (vehicle) (A and C) or 500 nM nocodazole (B and D) for 15 min and stained with anti-GFP and anti-α-tubulin antibodies. GFP-Capn6 induced thick microtubule bundling (C), which was resistant to the destabilizing effect of nocodazole (D). The scale bars indicate 20 μm.

antibody against a synthetic oligopeptide corresponding to the C-terminal region of Capn6. This antibody recognized a band of ~74 kDa, corresponding to the expected molecular mass of Capn6, in untransfected cell lysates and more strongly in Capn6-transfected cell lysates (Fig. 5A), although it also detected several additional bands of unknown origin. The specificity of this ~74-kDa band was also confirmed by RNAi-mediated knockdown (see Fig. 8B).

To characterize the nature of Capn6 in terms of microtubule association, cell lysates were subjected to crude fractionation and Western blotting. Although microtubules are prone to depolymerization in the presence of 0.1% NP-40 at low temperature, MAP4, a protein associated with cold-stable microtubules (40), and a portion of acetylated α-tubulin were detected in the insoluble fraction (Fig. 5B). Capn1, a classical calpain localized in the cytoplasm, was found only in the soluble fraction (Fig. 5B). Under these conditions, Capn6 was predominantly detected in the insoluble fraction (Fig. 5B), which is consistent with the idea that Capn6 may associate with microtubules.

Correspondingly, immunostaining of NIH 3T3 cells with anti-Capn6 antibody detected signals mainly in the cytoplasm in a filamentous pattern, at least partially (Fig. 5C). This fine structure did not correlate with actin microfilaments visualized by rhodamine-labeled phalloidin (data not shown) but was largely superimposed on the intracellular microtubule network detected by anti-α-tubulin antibody (Fig. 5C). The correlation between Capn6 and microtubule signals was intensified in the presence of the microtubule-stabilizing agent paclitaxel (Fig. 5D). Conversely, treatment with nocodazole caused loss of the filamentous pattern of immunostaining and disrupted the colocalization between Capn6 and microtubules (Fig. 5E). In contrast to the predominant distribution of Capn6 to microtubules, Capn1 was localized in the cytoplasm with a granular pattern, although the signals could be partially overlapped with microtubules (Fig. 5F).

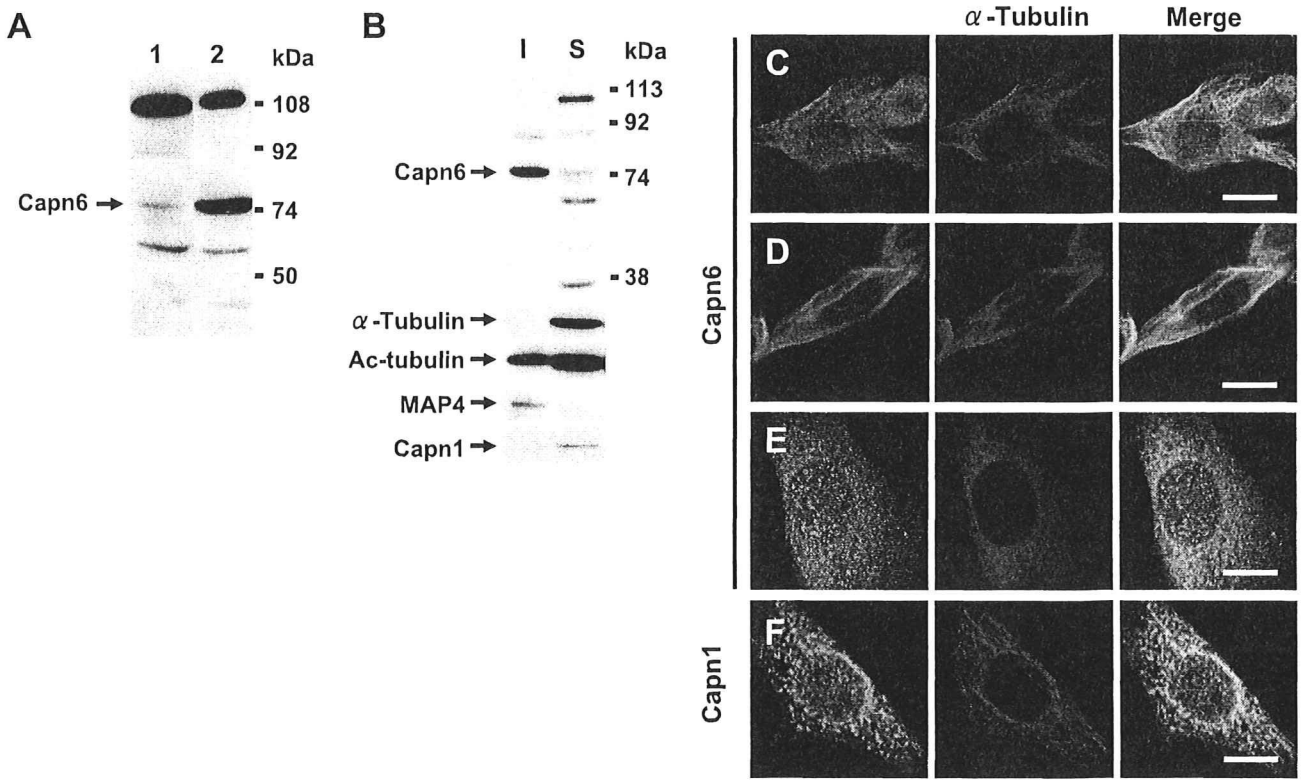

FIG. 5. Detection of Capn6 by rabbit polyclonal antibody. (A) Whole-cell lysates of untrasfected (lane 1) and Capn6-transfected (lane 2) NIH 3T3 cells were immunoblotted. The Capn6 antibody recognizes a band of ~74 kDa in untransfected cell lysates and more strongly in Capn6-transfected cell lysates. (B) NIH 3T3 cell lysates were separated into 0.1% NP-40-insoluble (lane I) and -soluble (lane S) fractions and immunoblotted with the indicated antibodies. The ~74-kDa band was found in the insoluble fraction with acetylated α-tubulin (Ac-tubulin) and MAP4. (C to F) Endogenous Capn6 colocalizes to the microtubule network. NIH 3T3 cells were treated with DMSO (vehicle) (C and F), 500 nM paclitaxel (D), or 500 nM nocodazole (E) for 30 min, and double stained with the anti-Capn6 (C to E) or anti-Capn1 (F) and anti-α-tubulin antibodies. The scale bars indicate 20 μm.

Capn6 interacts biochemically with microtubules. To test whether Capn6 can biochemically interact with microtubules, we performed a microtubule cosedimentation assay on NIH 3T3 cell lysate. After incubation of the cell lysate on ice for microtubule depolymerization, centrifugation yielded soluble supernatant containing monomerized tubulin. As shown in Fig. 6A, endogenous Capn6 was recovered in the microtubule-containing pellet in the presence of paclitaxel, although a large quantity of Capn6 remained in the supernatants. MAP4 also coprecipitated with microtubules in the pellet, whereas Capn1 remained in supernatants regardless of paclitaxel; these served as positive and negative controls, respectively (Fig. 6A). When GFP-Capn6 was overexpressed in NIH 3T3 cells, it was cosedimented with microtubules after the addition of paclitaxel, whereas it remained in the soluble fraction without paclitaxel treatment (Fig. 6B). In contrast, control GFP was not correlated with the amount of α-tubulin sedimented in the pellet, although a trace signal was detected in each lane (Fig. 6B).

The interaction between Capn6 and microtubules was further confirmed by a microtubule binding assay on filter paper and a GST pull-down assay. GST-Capn6 and unfused GST were run in SDS-PAGE, transferred to a PVDF filter, and then incubated with paclitaxel-stabilized microtubules. Immunoblotting with anti-tubulin antibody demonstrated that GST-Capn6, but not unfused GST, interacted with microtubules on the filter (Fig. 6C, lanes 1 and 2). MAP2, used as a positive control, also interacted with microtubules (Fig. 6C, lane 3). Furthermore, GST-Capn6, but not GST alone, pulled down paclitaxel-stabilized microtubules from NIH 3T3 cell lysates (Fig. 7C).

Domain III is responsible for Capn6-microtubule interaction. The structure of Capn6 protein consists of four domains (domains I, II, III, and T). To determine the domain(s) responsible for the interaction with microtubules, we constructed expression plasmids encoding GFP-tagged Capn6 deletion mutants (Fig. 7A) and transfected them into NIH 3T3 cells. In the presence of paclitaxel, GFP-tagged full-length Capn6 and Capn6(1-503), lacking domain T, colocalized to thickened microtubule bundles (Fig. 7B, a and b). In contrast, GFP-Capn6(1-326), lacking both domain III and domain T, did not colocalize to microtubules (Fig. 7B c). When individual domains were fused to GFP, only the construct containing domain III, GFP-Capn6(327-503), exhibited colocalization to microtubule bundles (Fig. 7B, d to g). Although domain III is sufficient for colocalization to microtubules, both 1-503 and 327-503 mutants did not induce multinucleation (data not shown), indicating that domain T is also necessary for full functional activity.

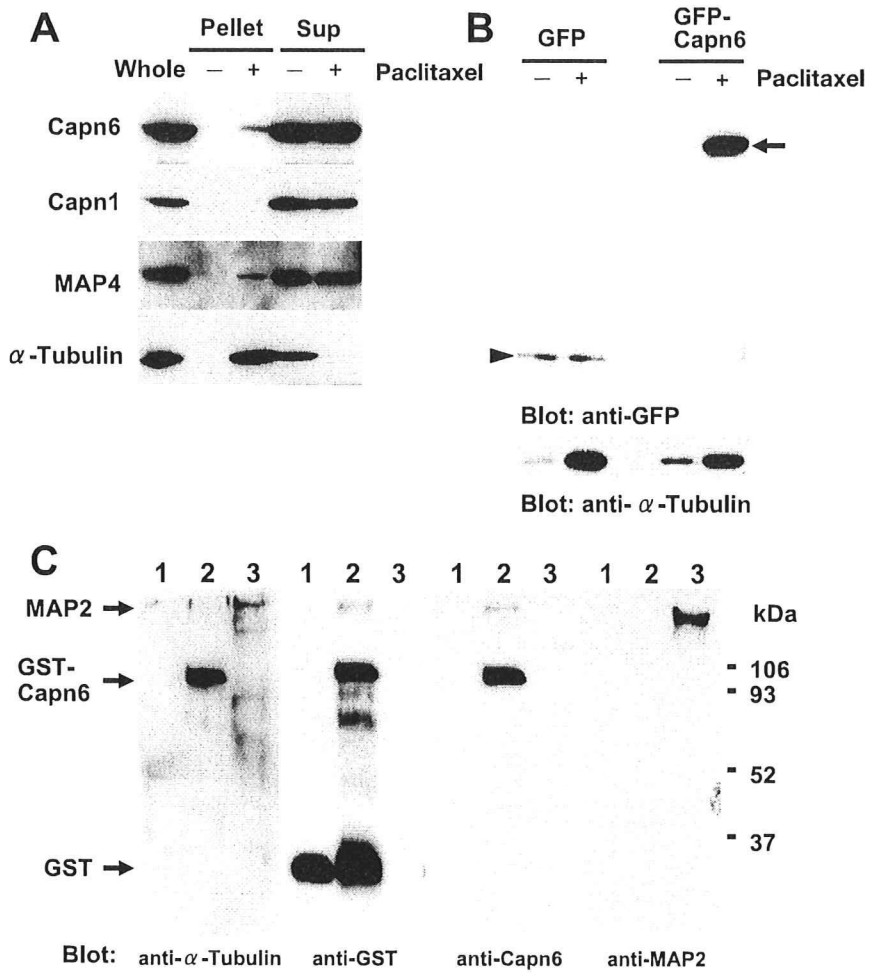

FIG. 6. Capn6 biochemically interacts with microtubules. (A and B) Lysates of untransfected (A) or GFP-Capn6-transfected (B) NIH 3T3 cells were subjected to microtubule cosedimentation assay. (A) Endogenous Capn6 was detected in the microtubule-containing pellet in the presence of paclitaxel, although a large quantity of Capn6 remained in the supernatants (Sup). MAP4 also coprecipitated with microtubules in the pellet, whereas Capn1, detected as autolytic products, remained in the supernatants regardless of the presence of paclitaxel. (B) Overexpressed GFP-Capn6 was recovered in the pellet in the presence of paclitaxel. In contrast, control GFP did not correlate with the amount of precipitated α-tubulin in the pellet. Arrow, GFP-Capn6; arrowhead, GFP. (C) Unfused GST (lane 1), GST fused to full-length Capn6 (lane 2), and purified MAP2 (lane 3) were subjected to a microtubule binding assay on filter paper. GST-Capn6 and MAP2 (positive control), but not unfused GST, bound to microtubules as detected by anti-α-tubulin antibody. The filter was sequentially reblotted with anti-GST, anti-Capn6, and anti-MAP2 antibodies to confirm the presence of intact proteins.

The association of each domain with microtubules was also examined by GST pull-down assay. GST-Capn6, but not unfused GST, pulled down paclitaxel-stabilized microtubules from NIH 3T3 cell lysates (Fig. 7C). Microtubules were also pulled down by GST-Capn6(327-503) (domain III) and GST-Capn6(504-641) (domain T), but not by GST-Capn6(1-56) (domain I) and GST-Capn6(57-326) (domain II) (Fig. 7C). Blotting with anti-acetylated α-tubulin revealed preferential binding of stabilized microtubules to domain III compared with domain T (Fig. 7C). These results suggest that the interaction of Capn6 with microtubules is mainly mediated by domain III, although domain T may also contribute to this association.

Suppression of Capn6 by siRNA destabilizes microtubules and affects actin organization. To investigate the role of endogenous Capn6 in the organization of the microtubule network, we used RNAi to selectively knock down Capn6 expression in NIH 3T3 cells. Stealth siRNAs targeting two different regions of the Capn6 transcript (nucleotides 1298 to 1322 and 1715 to 1739) downregulated Capn6 mRNA (Fig. 8A) and protein (Fig. 8B) to different extents. Immunostaining with anti-Capn6 antibody revealed the disappearance of microtubule-superimposed signals in Capn6-downregulated cells (Fig. 8C). In proportion to the extent of Capn6 downregulation, Capn6 siRNAs decreased the level of acetylated α-tubulin within the microtubule network of transfected cells (Fig. 8D). To confirm the effect of Capn6 downregulation on the microtubule organization, we introduced siRNAs into NIH 3T3 cells stably expressing GFP-tubulin. In Capn6 siRNA-transfected cells, the filamentous organization of the microtubule network was largely disrupted, resulting in relatively homogeneous distribution of GFP-tubulin with a preference for the perinuclear

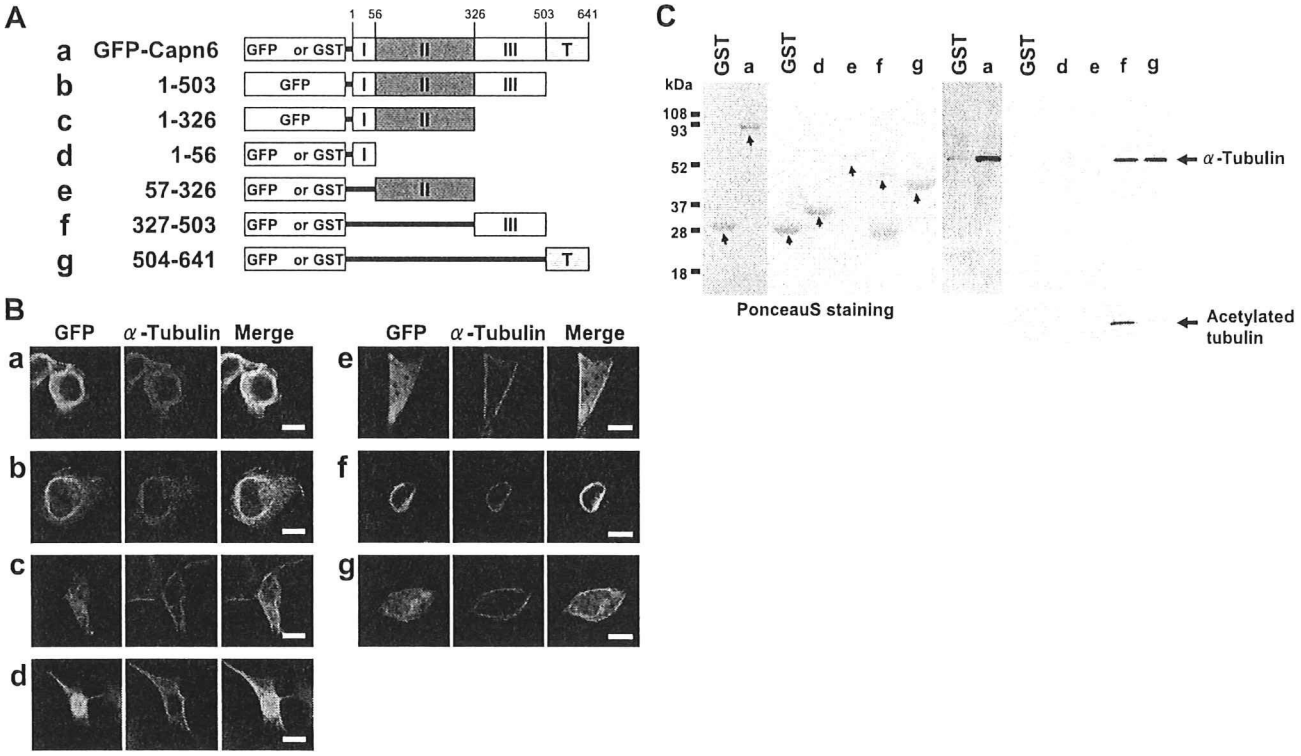

FIG. 7. Mapping of Capn6 domains interacting with microtubules. (A) Structures of GFP-tagged full-length Capn6 and its deletion mutants. (B) Localization of GFP-Capn6 mutants. NIH 3T3 cells were transfected with expression plasmids encoding GFP-Capn6 mutants, treated with 500 nM paclitaxel for 1 h, and stained with anti-GFP and anti-α-tubulin antibodies. Note that only GFP-Capn6 mutants containing domain III (amino acids 327 to 503) colocalized to microtubule bundles. The scale bars indicate 20 μm. (C) GST pull-down assay for microtubule binding. Microtubules were detected by anti-α-tubulin and anti-acetylated tubulin antibodies. α-Tubulin was pulled down from NIH 3T3 cell lysates by GST–full-length Capn6, GST-Capn6(327-503) (domain III), and GST-Capn6(504-641) (domain T), but not by GST-Capn6(1-56) (domain I), GST-Capn6(57-326) (domain II), or GST alone (right). Blotting with anti-acetylated tubulin showed that stable microtubules were more likely to bind to domain III than to domain T. The amounts of GFP fusion proteins were grossly estimated by Ponceau staining (left). The arrows indicate GST fusion proteins.

region (Fig. 8E). Decreases in acetylated-α-tubulin levels in Capn6-downregulated cells were also confirmed by Western blotting analysis (Fig. 8F).

To further analyze the functional consequences of Capn6 downregulation, we examined cellular behavior during cytokinesis in control and Capn6 siRNA-transfected cells using time-lapse microscopy. After the onset of anaphase, cleavage furrow formation and progression occurred normally in Capn6-downregulated cells, as well as in control cells (Fig. 9A and B). At subsequent stages, Capn6-downregulated cells tended to form lamellipodial protrusions with ruffling and to become flat much earlier than control cells (Fig. 9A and B). When the times from anaphase onset to the first appearance of lamellipodial protrusions from round dividing cells were compared, it was significantly shorter in Capn6-downregulated cells than in control cells (Fig. 9C). In contrast, the time from anaphase onset to the completion of cell abscission was not significantly different between control and Capn6-downregulated cells (Fig. 9D).

Time-lapse microscopy also showed that cell motility was increased in Capn6-downregulated cells, in which lamellipodial ruffling was very prominent (Fig. 10A and B; see Videos S4 to S6 in the supplemental material). Changes in actin organization associated with lamellipodium formation were confirmed by staining with rhodamine-phalloidin (Fig. 10C). These observations suggest that silencing of Capn6 may facilitate dynamic instability of microtubules and actin reorganization in NIH 3T3 cells.

DISCUSSION

In the present study, we first identified Capn6 as a downstream molecule of ET-1 signaling in pharyngeal-arch development. Subsequent analysis has demonstrated that Capn6 is a functional protein with microtubule-associated activities. Overexpression of Capn6 stimulated the formation of microtubule bundles and interrupted cytokinesis, resulting in multinucleation. Capn6 colocalized to the microtubule structures, including the central spindle and midbody, during cytokinesis. The interaction between Capn6 and microtubules was also confirmed by biochemical analysis. This interaction appeared to be mainly mediated by domain III, a C2-like domain. Finally, RNAi-mediated Capn6 inactivation caused disruption of the microtubule organization with loss of acetylated α-tubulin, affecting actin organization and cell motility.

Microtubules are filamentous polymers constituted of α- and β-tubulin that are engaged in many cellular functions, includ-

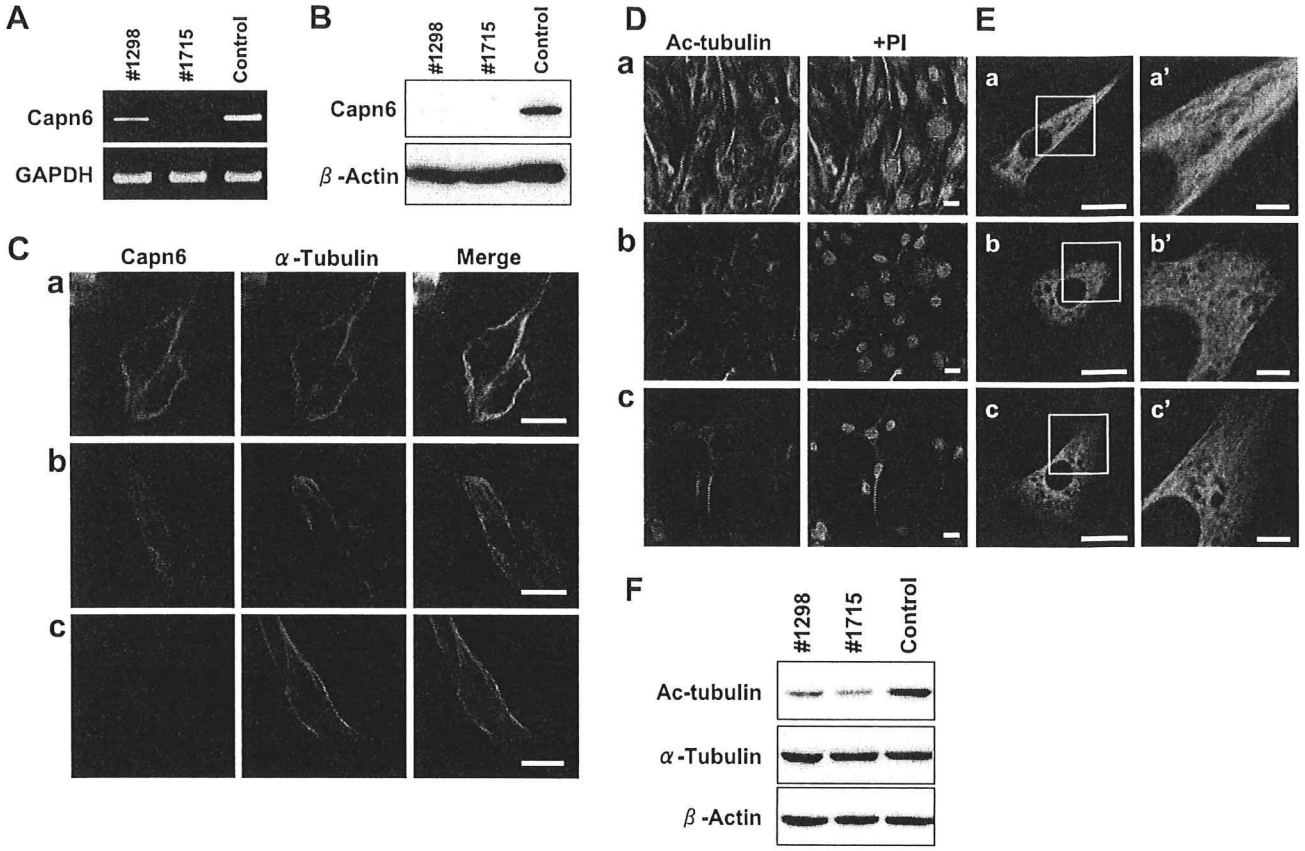

FIG. 8. RNAi-mediated inactivation of Capn6 destabilizes microtubules. NIH 3T3 cells were transfected with Capn6-targeted or control siRNAs. Forty-eight hours after transfection, the effects of siRNAs were evaluated. (A and B) RT-PCR for Capn6 mRNA (A) and Western blotting for Capn6 protein (B). Stealth siRNAs targeting two different regions of the Capn6 transcript (1298 and 1715 for nucleotides 1298 to 1322 and 1715 to 1739, respectively) downregulated Capn6 mRNA and protein levels. (C) Immunostaining with anti-Capn6 antibody. Signals superimposed on microtubules were evident in paclitaxel-treated control siRNA-transfected cells (a), but not in paclitaxel-treated cells transfected with 1298 (b) or 1715 (c) siRNA, although background cytosolic staining was comparable in the three groups. (D) NIH 3T3 cells were transfected with control (a), 1298 (b), or 1715 (c) siRNA and immunostained for acetylated α-tubulin (Ac-tubulin). The levels of acetylated α-tubulin decreased in cells transfected with Capn6-targeted siRNA. (E) NIH 3T3 cells stably expressing GFP-tubulin were transfected with control (a), 1298 (b), or 1715 (c) siRNA and immunostained for GFP. a′, b′, and c′ are magnified images of the boxed areas in a, b, and c, respectively. Microtubule network structures were largely disrupted in cells transfected with Capn6-targeted siRNA. The scale bars indicate 20 μm (C, D, and a to c in panel E) and 5 μm (a′ to c′ in panel E). (F) Western blotting of control and Capn6 siRNA-transfected NIH 3T3 cell extracts with anti-acetylated α-tubulin, anti-α-tubulin, and anti-β-actin antibodies. Acetylated α-tubulin levels decreased in Capn6 siRNA (1298 and 1715)-transfected cells compared with control siRNA-transfected cells, whereas total α-tubulin levels did not decrease. Blotting for β-actin served as an internal control. Similar results were obtained in three independent experiments. Representative data are shown.

ing cell division, cell shape integration, and organelle transport. The dynamic instability involving polymerization-depolymerization cycles is regulated by microtubule-associated proteins (MAPs), such as MAP1, MAP2, and tau, in neural cells and is critical for the function of microtubules. Many previous reports have demonstrated that the classical calpains can cleave tubulin and MAPs under in vitro conditions (11). However, little is known about the physiological role of the calpain system in the regulation of microtubule dynamics. Recently, several studies have implicated the calpain-induced proteolysis of MAPs in the pathogenesis of neurodegenerative disorders, including Alzheimer's disease (12), and the role of the calpain system in microtubule organization is now an issue of growing concern. In this context, the present findings may provide new insight into this issue by demonstrating that the protease-deficient calpain can associate with and stabilize microtubules.

Preferential distribution to the microtubule network is highly characteristic of Capn6 among the calpain family members. Capn1, for example, is homogeneously distributed in the cytoplasm and is translocated to the plasma membrane upon an increase in cytosolic Ca^{2+} (8). Lane et al. reported that Capn1 is distributed through the cytoplasm in a fibrillar form, reminiscent of the cytoskeletal architecture (24). In our present study, however, Capn1 was detected in the 0.1% NP-40-soluble fraction and distributed in a rather granular form in NIH 3T3 cells. Capn2, another classical calpain, also localizes in the cytoplasm in a diffuse or fine granular form (24). No other calpains have been shown to be associated with microtubules.

The interaction between Capn6 and microtubules appears to be mediated mainly by domain III. In Capn1 and Capn2, domain III constitutes a pair of four-stranded antiparallel

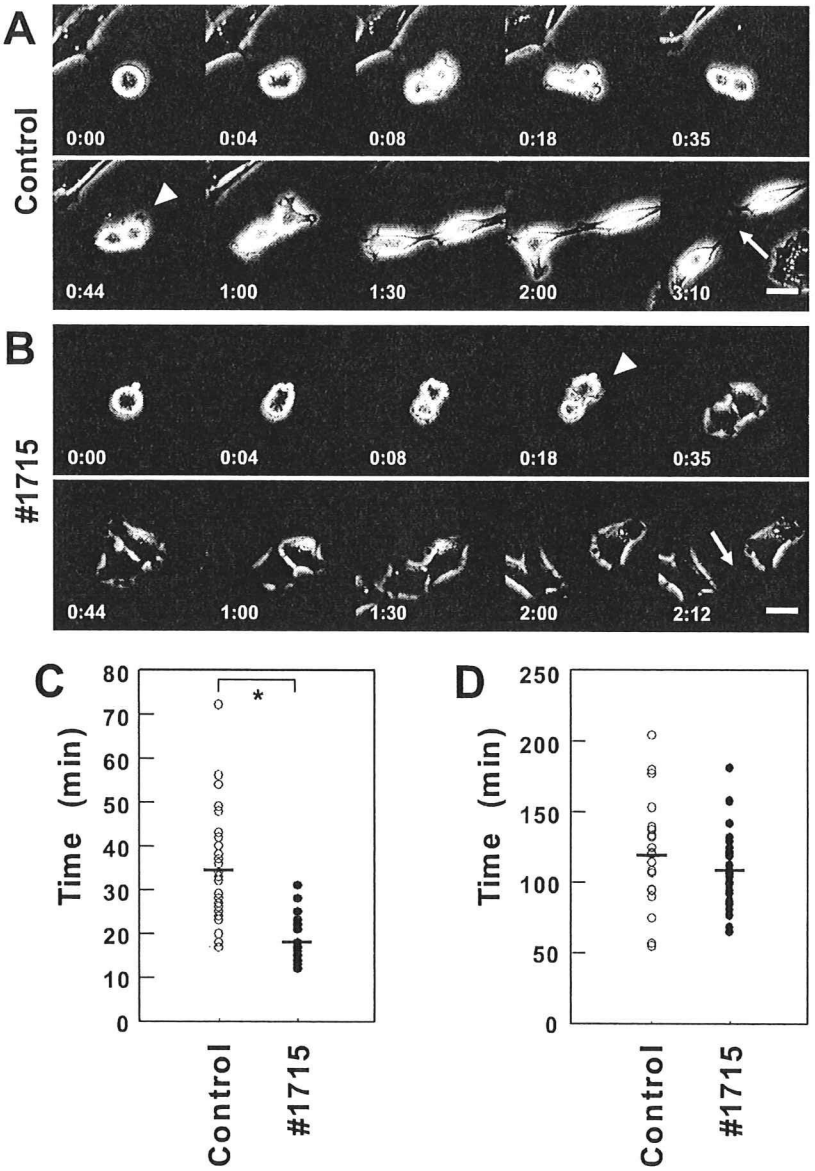

FIG. 9. RNAi-mediated inactivation of Capn6 affects cytoskeletal reorganization during cytokinesis. (A and B) Representative images from time-lapse recordings of control (A) and Capn6 (B) siRNA-transfected NIH 3T3 cells. Cleavage furrows were similarly formed after anaphase onset in control and Capn6 siRNA (1715)-transfected cells. At subsequent stages, Capn6 siRNA-transfected cells tended to form lamellipodial protrusions with ruffling and to become flat much earlier than control cells. Times are in h/min after anaphase onset (0:00 time point). Arrowheads, first appearance of lamellipodial protrusion; arrows, completion of cell abscission. The scale bars indicate 20 μm. (C) Comparison of the times from anaphase onset to the first appearance of lamellipodial protrusions. The time was significantly shorter in Capn6-downregulated cells (17.9 [mean] ± 4.5 [standard deviation] min; $n = 30$) than in control cells (34.4 ± 12.4 min; $n = 30$). *, $P < 0.0001$; Mann-Whitney nonparametric test. (D) Comparison of the times from anaphase onset to the completion of cell abscission. No significant difference was observed between control cells (118.8 ± 35.1 min; $n = 25$) and Capn6-downregulated cells (108.6 ± 27.6 min; $n = 24$).

β-sheets (15, 30, 37), like the C2 domain, a Ca^{2+}- and phospholipid-binding module (33). Although the function of this domain is unclear, previous reports have indicated its roles in the regulation of Ca^{2+} sensitivity of the enzyme (14, 15) and in Ca^{2+}-dependent translocation to the cell membrane (8). Domain III of Capn6 (amino acids 327 to 503) shows similarity to that of Capn2, with only 28% amino acid identity, as revealed by a BLAST search (data not shown), suggesting limited conservation of the domain structure. In addition, domain III of Capn6 lacks sequences corresponding to the conserved acidic loop to form interdomain salt bridges important for Ca^{2+} sensitivity (13). Thus, this domain may be unusual in structure and function in the calpain family.

In addition to colocalization to microtubules, Capn6 causes the formation of microtubule bundles. Increased acetylated α-tubulin contents in Capn6-induced microtubule bundles and resistance to nocodazole suggest that Capn6 has a microtubule-stabilizing property. Furthermore, disruption of microtu-

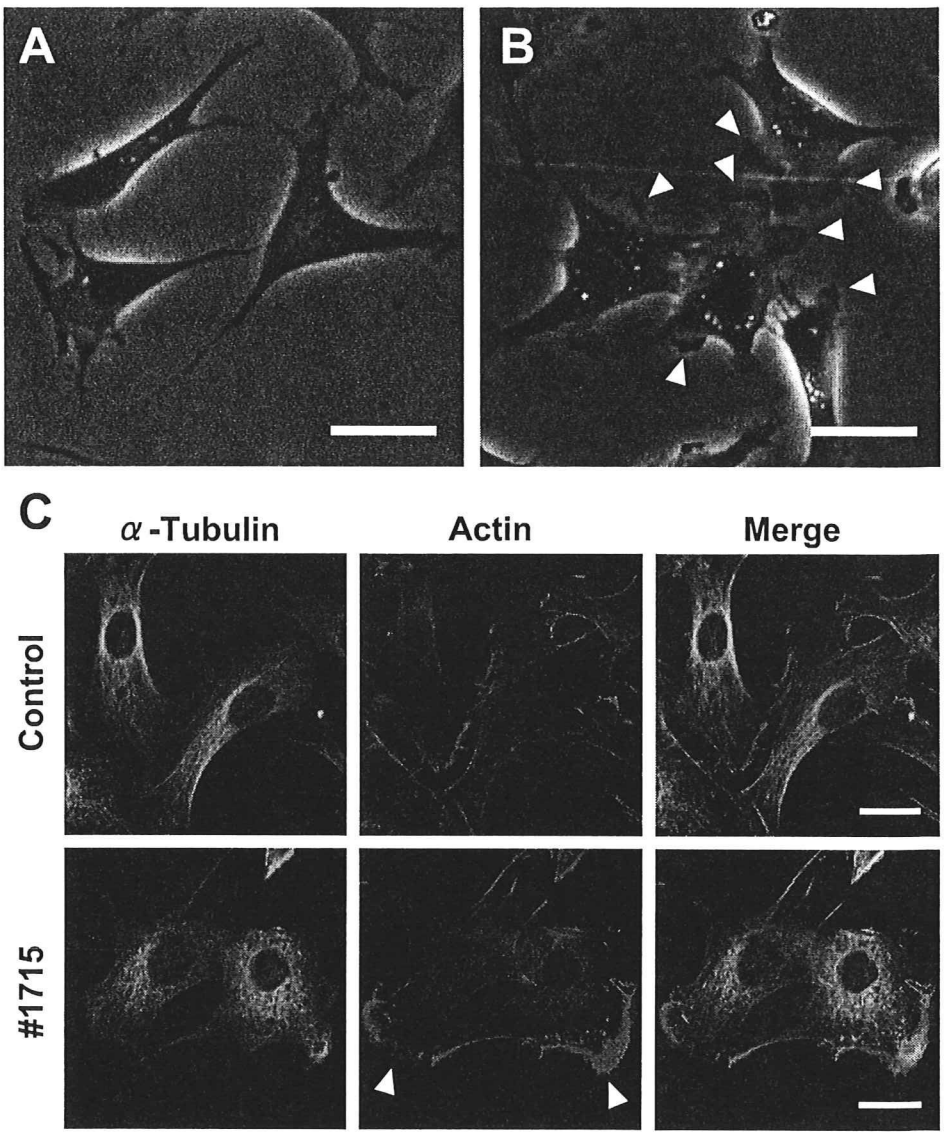

FIG. 10. RNAi-mediated inactivation of Capn6 induces lamellipodium formation. (A and B) Phase-contrast micrographs of control (A) and Capn6 (B) siRNA-transfected NIH 3T3 cells. Capn6 siRNA(1715)-transfected cells demonstrated enhanced lamellipodium formation with membrane ruffling (arrowheads). (C) Double staining of control and Capn6(1715) siRNA-transfected NIH 3T3 cells with anti-tubulin and rhodamine-phalloidin. Capn6 siRNA-transfected cells demonstrate the assembly of actin filaments in lamellipodia (arrowheads). The scale bars indicate 20 μm.

bule bundles and decrease in acetylated α-tubulin levels by RNAi-mediated Capn6 inactivation indicate the role of endogenous Capn6 in the maintenance of stable microtubule architecture.

The Capn6-induced disruption of cytokinesis may be a consequence of its stabilizing effect on microtubules. In Capn6-overexpressing cells, the cleavage furrow was created along with chromosomal separation with an expected time course, but furrow ingression was retarded thereafter, suggesting that Capn6 functioned at the late stage of cytokinesis. During the process of cytokinesis, overexpressed Capn6 colocalized to the central spindle of the midzone and to the whole midbody, where Capn6 may affect the progression and completion of cytokinesis. Cytokinesis is elaborately controlled at several steps involving various molecules concentrating at the midbody (10). Changes in microtubule stability might interrupt such cytokinetic machinery, leading to disrupted cytokinesis in Capn6-overexpressing cells. Another possible explanation is that stabilization of microtubules by Capn6 may prevent the cytoskeletal reorganization required for cell division, although the molecular network underlying this process remains largely unknown. Correspondingly, Capn6 siRNA transfection resulted in the early appearance of lamellipodial protrusions during cytokinesis, indicating that cytoskeletal reorganization may be facilitated by Capn6 inactivation.

The observation that siRNA-mediated Capn6 inactivation